Growth of the Lesser Himalayan Duplex and rapid fluvial incision modulate landscape morphology in tectonically-active Kishtwar Window in NW Himalayan interiors

Saptarshi Dey[1], Rasmus Thiede[2], Arindam Biswas[3], Naveen Chauhan[4], Pritha Chakravarti[1], and Vikrant Jain[1]

[1]*Earth Science Discipline, IIT Gandhinagar, Gandhinagar-382355, India.*

[2]*Institute of Geosciences, Christian Albrechts University of Kiel, Kiel-24118, Germany.*

[3] *Department of Applied Geology, IIT-ISM Dhanbad, Jharkhand-826004, India.*

[4] *Atomic Molecular and Optical Physics Division, Physical Research Laboratory, Ahmedabad.*

Corresponding author

Saptarshi Dey

saptarshi.dey@iitgn.ac.in

Abstract

The Kishtwar Window (KW) of the NW Himalaya exposes the north-western termination of the orogen-parallel anticlinal stack of thrust nappes, known as the Lesser Himalayan Duplex. However, its exact tectonic deformation pattern, geographic extent and activity are still debated. Here we combine morphometric analyses with structural data, field evidence and chronological constraints to describe the spatial pattern of internal deformation of the duplex. We agree with previous findings that the variations in the geometry of the basal décollement, the Main Himalayan Thrust (MHT) is important; however, the observed topography and neotectonic deformation can be explained only with additional internal faulting within the duplex. We recognize two significant steep stream segments/ knickzones, one in the center of the window, and a second one along its western margin, which we relate to fault-ramps emerging from the MHT. The larger of the knickzones corresponds tohighly-fractured and folded rocks at the base of the steep stream segment suggesting internal deformation of the duplex, possibly linked to surface-breaking thrust fault-ramp at the core of the duplex. The second steepened knickzone coincides with the western margin of the window and is identified by a narrow channel through a comparatively weaker bedrock gorge. Luminescence dating of sediments overlying the bedrock strath provides the upper limit of terrace abandonment. We deduced a minimum of 3.1-3.5 mm/y fluvial bedrock incision on the MHT-fault ramp which is in overall agreement with long-term exhumation rates from the KW. Summarizing our findings, we favor a structural and active tectonic control on the growth of the duplex even over geomorphic timescales.

Keywords

Steepness index, knickzone, rock strength, Lesser Himalayan Duplex, Main Himalayan Thrust.

1. Introduction

Protracted convergence between the Indian and the Eurasian plate resulted into the growth and evolution of the Himalayan orogen and temporally in-sequence formation of the Southern Tibetan Detachment System (STDS), the Main Central Thrust (MCT), the Main Boundary Thrust (MBT) and the Main Frontal Thrust (MFT) towards the south (Yin and Harrison, 2000; Yin, 2006; Mukherjee, 2013). All these fault-zones emerge from a low-angle basal decollement, viz. the Main Himalayan Thrust (MHT) which forms the base of the Himalayan orogenic wedge (Ni and Barazangi, 1984; Nabelek et al., 2009; Avouac et al., 2016). The MHT was probably established in the late Miocene (Vannay et al., 2004).

The majority of scientists have favored that the late Pleistocene-Holocene shortening is mostly accommodated within the southern fringe of the Himalayan wedge, i.e., the Sub-Himalaya (morphotectonic segment in between the MBT and the MFT) (Wesnousky et al., 1999; Lave and Avouac, 2000; Burgess et al., 2012; Thakur et al., 2014; Mukherjee, 2015; Vassalo et al., 2015; Dey et al., 2016; Dey et al., 2019). This implies that the northerly thrusts, i.e., the MBT and the brittle faults exposed in the vicinity of the southern margin of the Higher Himalaya, are considered inactive over millennial timescales. However, in recent years, several studies that focused on the low-Temperature thermochronologic data and thermal modeling of the interiors of the NW Himalaya have raised questions on this. The recent studies suggested that 10-15% of the total Quaternary shortening has been accommodated within the interiors of the Himalaya as out-of-sequence deformation (Thiede et al., 2004; Deeken et al., 2011; Thiede et al., 2017; Gavillot et al., 2018) (Supplementary Fig. B1). Earlier, out-of-sequence deformation of the Himalayan wedge has been explained

by two end-member models- (a)the reactivation of the MCT (Wobus et al., 2003), or, (b) enhanced rock uplift over a major ramp on the MHT (Bollinger et al., 2006; Herman et al., 2010; Robert et al., 2009). Landscape evolution models, structural analysis and thermochronologic data from the interior of the Himalaya favor that the Lesser Himalaya has formed a duplex at the base of the southern Himalayan front by sustained internal deformation since late Miocene (Decelles et al., 2001; Mitra et al., 2010; Robinson and Martin, 2014). The growth of the duplex resulted in the uplift of the Higher Himalaya and established the major topographic and orographic barrier as seen today. The Kishtwar Window (KW) in the NW Himalaya represents the north-western termination of the Lesser Himalayan Duplex (LHD). While most of the published cross-sections of the Himalayan orogen today recognize the duplex (Webb et al., 2011; Mitra et al., 2010; DeCelles et al., 2001), usually very little or no data is available whether the duplex is active over millennial timescales, and potentially a source of major Holocene earthquakes.

The pioneering low-temperature thermochron study by Kumar et al. (1995) portrayed the first orogen-perpendicular sampling traverse extending from the south-western margin of the Kishtwar tectonic Window crossing the Zanskar Range. More recent studies link the evolution of the KW to the growth of the LHD (Gavillot et al., 2018). Along its margin, it is surrounded by the Miocene MCT shear zone along the base of the High Himalayan Crystalline Sequence (HHCS). Locally, the bounding fault zone is named the Kishtwar Thrust (KT). Thermochronological constraints suggest higher rates of exhumation within the KW (3.2-3.6 mm/y) (Gavillot et al., 2018). Their findings corroborate well with similar thermochron-based Quaternary exhumation rates published from the of the Kullu-Rampur window in eastern Himachal Pradesh((Jain et al., 2000; Vannay et al., 2004; Thiede et al., 2004; Stübner et al., 2018). In contrast, geodetic shortening rates lack spatial resolution and only capture inter-seismic deformation (Banerjee and Burgmann, 2002; Kundu et al., 2014),

and there exists no chronological data to provide information on ongoing tectonic activity in the interiors of the Himalaya over intermediate timescales. Therefore, to understand the 10^3-10^4-year timescale neotectonic evolution, either we have to have geological field evidence, chronologically-constrained geomorphic markers or at least have a rigorous morphometric analysis of potential study areas, such as the KW.

In this study, we will focus on a few long-standing questions on Himalayan neotectonic evolution, which are-

1. What is the spatial extent of neotectonic deformation, if any, in the interiors of the Himalaya?

2. What is the role of the Lesser Himalayan duplex in defining the morphology of the Himalayan interiors?

3. How reliably can we infer about sub-surface structural variations of the orogenic wedge by analyzing the terrain morphology?

4. Can we obtain new constraints on deformation over millennial timescales? Do millennial-scale fluvial incision rates support long-term exhumation rates?

To address these questions, we adopted a combination of methods such as morphometric analysis using high-resolution digital elevation models, field observation on rock type, structural variations as well as rock strength data and analysis of satellite images to determine channel width and assessing the spatial distribution and relative differences in the late Quaternary deformation of the KW and surroundings (Fig.1). We aimed to test if the landscape morphology can be explained by changes in the geometry of the basal decollement. We used basinwide steepness indices and specific stream power calculation (derived from

channel gradient and channel width) as a proxy of the fluvial incision. And, lastly but most importantly, we calculated the fluvial bedrock incision rates by using depositional ages of aggraded sediments along the Chenab River. In this study, we show that the regional distribution of faulting is concentrated in the core and along the western margin of the window. We propose that active faulting within the LH Duplex is controlling the ongoing deformation in the Himalayan interior and driving the uplift of Higher Himalaya in its hanging wall. Our new estimates on the bedrock incision rate agree with Quaternary exhumation rates from the KW, which mean consistent active growth of the duplex over million-year to millennial timescales.

2. Geological background and field observations

The orogenic growth of the Himalaya is defined by overall in-sequence development of the orogen-scale fault systems which broadly define the morphotectonic sectors of the orogen (Fig. 1b). Notable among those sectors, the Higher Himalaya is bordered by the MCT in the south and is comprised of high-grade metasediments (Haimanta Formation), Higher Himalayan Crystalline Sequence (HHCS), and Ordovician granite intrusives (Yin and Harrison, 2000). The Low-grade metasediments (quartzites, phyllites, schists, slates) of the Proterozoic Lesser Himalayan sequence are exposed between the MCT in the north and MBT in the south. The Lesser Himalayan domain is narrow (4-15 km) in the NW Himalaya except where it is exposed within tectonic windows (Kishtwar window, Kullu-Rampur window etc.) (Steck, 2003). The Sub-Himalayan fold-and-thrust belt lying to the south of the MBT is tectonically the most active sector since the late Quaternary (Thakur et al., 2014; Vignon et al., 2016).

Near the southwest corner of our study area, Proterozoic low-grade Lesser Himalayan metasediments are thrust over the Tertiary Sub-Himalayan sediments along the MBT (Wadia, 1934; Thakur, 1992). Near the Chenab region, Apatite U-Th/He ages suggest that cooling and exhumation related to faulting along the MBT thrust sheet initiated before ~5 ± 3 Myr (Kumar et al., 1995). Geomorphic data obtained across the MBT in Kashmir Himalaya suggest that MBT has not been reactivated for the last 14-17 ky (Vassallo et al., 2015). In the NW Himalaya, the Lesser Himalayan sequence (LHS) exposed between the MBT and the MCT is characterized by a < 10 km-wide zone of sheared schists, slates, quartzites, phyllites and Proterozoic intrusive granite bodies (Bhatia and Bhatia, 1973; Thakur, 1992; Steck, 2003). The LHS is bounded by the MCT shear zone in the hanging wall. The MCT hanging wall forms highly deformed nappe exposing lower and higher Haimantas, which are related to the Higher Himalayan Crystalline Sequence (HHCS) (Fig.2a) (Bhatia and Bhatia, 1973; Thakur, 1992; Yin and Harrison, 2000; Searle et al., 2007). Nearly 40 km NE of the frontal MCT shear zone, the MCT fault zone is re-exposed in the vicinity of KW and is called the Kishtwar Thrust (KT) (Ul Haq et al., 2019) (Fig. 1a, 2b). Within the KW, Lesser Himalayan Rampur quartzites (Fig.2c), low-grade mica schists and phyllites along with the granite intrusives are exposed (Steck, 2003; DiPietro and Pogue, 2004; Yin, 2006; Gavillot et al., 2018).KW exposes a stack of LHS nappes in the footwall of the MCT (in this case, KT) which is related to the Lesser Himalayan Duplex (LHD), characteristic of the central Himalaya (Decelles et al., 2001). Regionally balanced cross-sections (DiPietro and Pogue, 2004; Searle et al., 2007; Gavillot et al., 2018) suggest that the Himalayan wedge is bounded at the base by a low-angle décollement, namely as the MHT. Sub-surface structural formations beneath the KW are not well-constrained. A recent study by Gavillot et al. (2018) propose the existence of two mid-crustal ramp segments beneath the KW, viz., MCR-1 and MCR-2 (Fig. B2). Based on thermochronological constraints, Gavillot et al. (2018) and

Kumar et al. (1995) proposed that the core as well as the western margin of the window exhumed with rates ~ 3.2-3.6 mm/y during the Quaternary, at a higher rate when compared to the surroundings.

The Higher Himalayan sequence dips steeply away from the duplex (~65° towards west) (Fig.2a). The frontal horses of the LH duplex expose internally-folded greenschist facies rocks. Although at the western margin of the duplex, the quartzites stand sub-vertically (Fig.2b), the general dip amount reduces as we move from west to east for the next ~10-15 km up to the core of the KW. Near the core of the KW, we observed highly-deformed (folded and multiply-fractured) quartzite and granites at the core of the KW (Fig.2d, 2e). We also observed deformed quartz veins of at least two generations, as well as macroscopic white mica. Here, the River is also very steep and narrow; the rock units are also steeply-dipping towards the east (~55-65°) and are nearly isoclinal and strongly deformed at places (Fig.2f). Towards the eastern edge of the window, however, the quartzites dip much gently towards the east (~20-30°), and much lesser folding and faulting have been recognized in the field (Fig.2g).

The broad, ‘U-shaped’ valley profile near the town of Padder at the eastern margin of the KW is in contrast with the interior of the window (Fig.3a). At the core of the KW, the Chenab River maintains a narrow channel width and a steep gradient (Fig.3b). The E-W traverse of the Chenab River through the KW is devoid of any significant sediment storage. However, along the N-S traverse parallel to the western margin of the KW, beneath the Kishtwar surface, ~150-170m thick sedimentary deposits are transiently-stored over the steeply-dipping Higher Himalayan bedrock (Fig.3c). The height of the Kishtwar surface from the Chenab River is ~450m, which means ~280m of bedrock incision by the River since the formation of the Kishtwar surface. Along the N-S traverse of the River, epigenetic gorges are formed as a result of the damming of paleo-channel by the hillslope debris flow, followed by

the establishment of a newer channel path (Ouimet et al., 2008; Kothyari and Juyal, 2013). One example of such epigenetic gorge formation near the town of Drabshalla is shown in Fig.3d. Downstream from the town of Drabshalla, the River maintains narrow channel width (< 25 m) and flows through a gorge having sub-vertical valley-walls (Fig.3e). The tributaries originating from the Higher Himalayan domain form one major knickpoint close to the confluence with the trunk stream (Fig.3f). We have identified at least three strath surface levels above the present-day river channel, viz., T1 (280±5 m), T2 (170-175 m) and T3 (~120±5 m), respectively (Fig.3g). The first study on sediment aggradation in the middle Chenab valley (transect from Kishtwar to Doda town) was published by Norin (1926). He argued the sediment aggradation in and around the Kishtwar town is largely contributed by fluvioglacial sediments and the U-shaped valley morphology is a marker of past glacial occupancy. In general, we agree with the findings of Norin (1926) and Ul Haq et al., (2019) as we observe ~100m thick late Pleistocene fluvioglacial sediment cover unconformably overlying the Higher Himalayan bedrock, most likely to be paleo-strath surface (Fig.4b). At the same time, we do not agree with the interpretation of surface-breaking faults near Kishtwar town by Ul Haq et al. (2019). We inspected the proposed fault locations in detail and didn't find any indication of fault movement, including offset, broken and rotated clasts, fault gouges etc. on the proposed fault planes. Therefore, we refute the existence of such surface-breaking faults. The fluvioglacial sediments included alternate layers of pebble conglomerate and coarse-medium sand (Fig.4c). The pebbles are moderately rounded and polished suggesting significant fluvial transport. Our field observations suggest that the fluvioglacial sediments have been succeeded by a significant volume of hillslope debris (Fig.4c). The thickness of the debris-flow deposits is variable. The hillslope debris units contain mostly coarse-grained, highly-angular, poorly-sorted quartzite clasts from the frontal horses of the Lesser Himalayan Duplex. The hillslope debris units also contain a few fine-

grain sediment layers trapped in between two coarse-grained debris layers (Fig.4e). The town of Kishtwar is situated on this debris flow deposit.

3. Methods of morphometric analysis and field data collection

3.1.Morphometry

For conducting the morphometric analysis, we have used 12.5m ALOS-PALSAR DEM data (high resolution terrain-corrected) (Fig.5a). This DEM data has lesser issues with artifacts and noises than 30m SRTM data, which fails to capture the drainage network properly in areas populated by narrow channel gorges. We compiled the topographic relief over a circular moving window of 4 km diameter (Fig.5b) and the rainfall distribution of the Chenab region (Fig.5c). The rainfall distribution is adapted from 12-year-averaged annual rainfall data from TRMM database (Bookhagen and Burbank, 2006).

3.1.1. Basinwide normalized steepness indices

Global observations across a broad spectrum of tectonic and climatic regimes have revealed a power-law scaling between the local river gradient and upstream contributing area:

$$S = k_s . A^{-\theta} \qquad (1)$$

where S is the stream gradient (m/m), k_s is the steepness index ($m^{2\theta}$), A is the upstream drainage area (m^2), and θ is the concavity index (Flint, 1974; Whipple and Tucker, 1999). Normalized steepness-index values (k_{sn}) are steepness indices calculated using a reference concavity value (θ_{ref}), which is useful to compare steepness-indices of different river systems (Wobus et al., 2006). We extracted the k_{sn} values in the study area using the ArcGIS and MATLAB-supported Topographic Analysis Toolkit (Forte and Whipple, 2019) following the procedure of Wobus et al. (2006). We performed an automated k_{sn} extraction using a critical area of 10^6 m^2 for assigning the channel head, a smoothing window of 500 m, a θ_{ref} of 0.45,

and an auto-k_{sn} window of 250 m for calculating k_{sn} values. Stream-specific ksn values in and around the KW are drafted in Supplementary Fig.B3. The catchments were delineated by using a maximum threshold of 200 sq. km, so that the basins we pick are smaller in size. The stream-specific k_{sn} values were rasterized in ArcGIS and were extrapolated to the respective catchments using the zonal statistics toolbox. Basinwide mean k_{sn} values for the delineated watersheds are portrayed in Fig.5d.Basinwide mean k_{sn} values are plotted using a 500 km^2 threshold catchment area (Fig. 2d).

A 50-km-wide swath profile along line AB (cf.Fig.5a) show variation in elevation, mean annual rainfall and mean k_{sn} values in the area (Fig.2e).

3.1.2. Drainage network extraction

The drainage network and the longitudinal stream profiles were extracted using the Topographic Analysis Kit toolbox (Forte and Whipple, 2019). An equivalent of 20-pixel smoothing of the raw DEM (250 m smoothing window) data has been applied to remove noises from the DEM (Fig.6). The longitudinal stream profile of the Chenab trunk stream was processed with the Topotoolbox 'Knickpointfinder' tool (Schwanghart and Scherler, 2014). Several jumps/ kinks in the longitudinal profile are seen and those are marked as knickpoints (Fig.6). A 30m tolerance threshold was applied to extract only the major knickpoints. Results from knickpointfinder tool were rechecked with chi vs. elevation distribution (Supplementary Fig.B4). Identification of the knickpoints/ knickzones and their relationship with the rock-types as well as with existing structures are necessary to understand the causal mechanism of the respective knickpoints/ knickzones. Knickpoints/(zones) can be generated by lithological, tectonic and structural control. Lithological knickpoints are stationary and anchored at the transition from the soft-to-hard substrate. The tectonic knickpoints originate at the active tectonic boundary and migrate upstream with time. Structural variations, such as ramp-flat

geometry of any emerging thrust may cause a quasistatic knickpoint at the transition of the flat-to-ramp of the fault. In such cases, the ramp segment is characterized by higher steepness than the flat segment and often the ramp is characterized by a sequence of rapids, forming a wide knickzone, instead of a single knickpoint.

Longitudinal profile of the entire Himalayan traverse of the Chenab River show oversteepening across the KW (Fig.6), therefore, we focused on that segment (marked by red rectangle, cf. Fig.6) for further analysis. Longitudinal profile of the selected segment is shown in Fig.7a.

3.1.3. Channel Width

Channel width is a parameter of assessment of lateral erosion/incision through bedrocks of equivalent strength (Finnegan et al., 2005; Turowski, 2009). The channel width of the Chenab trunk stream within the elevation range of 600 to 2200 m above the MSL was derived by manual selection and digitization of the channel banks using the Google Earth Digital Globe imagery (http://www.digitalglobe.com/) of minimum 3.2 m spatial resolution. We used the shortest distance between the two banks as the channel width and rejected areas having largely unparallel channel-banks as that would bias the result. We used a 100 m step between two consecutive points for channel width determination. Ten point-averaged channel width data along with elevation of the riverbed is shown in Fig.7b. Variations in channel gradient and k_{sn} values along the longitudinal profile of the selected stretch are shown in Fig.7c and 7d, respectively.

3.1.4. Specific stream power (SSP) calculation

Specific stream power has often been used as a proxy of fluvial incision or differential uplift along the channel (Royden and Perron, 2013; Whipple and Tucker, 1999). Areas of higher uplift/incision are characterized by a transient increase in the specific stream power. Channel

slope and channel width data were used to analyze the corresponding changes in the specific stream power (SSP) from upstream of the gorge area to the gorge reaches (Bagnold, 1966). The SSP (ω) was estimated using the following equation –

$$\omega = \gamma . Q . s/w \qquad \text{(Eq. 1)}$$

Where, γ - unit weight of water, Q – water discharge, s – energy slope considered equivalent to the channel slope; w – channel width. With the available TRMM data, we argue that the rainfall distribution in the study area is almost uniformly low (<1.5 m/y) (Fig.5c and 5e) and therefore, we assumed a uniform discharge (Q) for SSP calculation. SSP data from selected stretches (stretch 1 and stretch 2, cf. Fig.8a) are shown in Table 1.

3.2. Field data collection

3.2.1. Structural data

We measured the strike and dip of the foliations and bedding planes of the Lesser and Higher Himalayan rocks using the Freiberg clinometer compass. We took at least five measurements at every location, and the average has been reported in Fig. 8a. Field photos in Fig.2 document the observed variations in the structural styles.

3.2.2. Rock strength data

Recording rock strength data in the field is essential to understand the role of variable rock-type and rock-strength in changes in morphology. It provides us vital insights on the genesis of knickpoints, whether they are lithologically-controlled or not. It also helps to understand the variations in channel steepness across rocks of similar lithological strength. We systematically measured the rock strength of the major geologic units using a hand-held rebound hammer. Repeated measurements (8-10 measurements at each of the 75 locations throughout the study area) were conducted to measure the variability of rock-strength within the major lithologic units. All the measurements were taken perpendicular to the bedding/

foliation plane, and no measurements are from wet surfaces or surfaces showing fractures. Each reading was taken at least 0.5m apart from the previous one. Average rock strength data collected from each of the test locations are plotted against the longitudinal river profile and channel width data in Fig.7e. Our data from individual sites are smaller in number than what is preferred for checking the statistical robustness of Schmidt hammer data (Niedzielski et al., 2009). Therefore, we combined the data from all sites representing similar lithology and portrayed the mean ±standard deviation for the same. Field data provided in Supplementary Table C1.

3.3. Luminescence dating of transiently-stored sediments in and around Kishtwar

Luminescence dating of Quaternary fluvial sediments is a globally accepted method for constraining the timing of deposition of sediments in a drainage system (Aitken, 1992; Olley et al., 1998; Wallinga et al., 2001; Cunningham and Wallinga, 2012). Although there exists a few persistent problems in luminescence dating of the Himalayan sediments (including low sensitivity of quartz and numerous cases of heterogeneous bleaching of the luminescence signal), studies over the past couple of decades have also provided an adequate control on Himalayan sedimentary chronology by using luminescence dating with quartz (Optically stimulated luminescence, OSL) and feldspar (Infra-red stimulated luminescence, IRSL). Earlier studies have reported sediment aggradation over the Higher Himalayan bedrocks in the Kishtwar valley (Norin, 1926; Ul Haq et al., 2019).

The samples for luminescence dating were collected in galvanized iron pipes. The pipes were opened in subdued red light (wavelength ~650 nm). The outer ~3 cm of sediment from both the ends of the pipe were removed to omit the possibility of exposure of the sample to daylight during collection. The removed portion was used for moisture content estimation and determination of Uranium (U), Thorium (Th), and Potassium (K) concentrations. The unexposed interior portion of the sample was further processed to obtain quartz and feldspar

using standard procedures (e.g., Aitken, 1998). The portion was treated with a sufficient quantity of 1N HCl and 30% H_2O_2 to remove carbonates and organic materials, respectively. The sediments were then oven-dried at 45°C and sieved to obtain a size fraction of 90-150 μm. The quartz and feldspar were separated using Frantz isodynamic separator at a magnetic field of ~10,000 gauss and collected separately. Obtained quartz grains were etched with 40% HF for 80 minutes to remove alpha irradiated outer layer (~10 μm), followed by 37% HCl treatment for 20 minutes to dissolve fluorides formed during the previous step. The isodynamic separation procedure was repeated to remove any broken feldspar grain. However, even after repeating the last step twice, we were unable to eliminate the feldspar contamination from most of the samples thoroughly. Those samples are not suitable for OSL SAR protocol.

Samples K02 and K11 procured from the fine-grain layers of ~1-1.5m thickness, trapped within coarse, angular and poorly-sorted thick layers of clasts (identified as hillslope debris) were used for OSL (Optically stimulated luminescence) dating using Double SAR (Single Aliquot Regenerative) protocol (IRSL wash before OSL measurement) for equivalent dose estimation (Roberts, 2007). The test doses were set for 75 Gy, 225 Gy, and 450 Gy, respectively (Fig.5). The aliquots were considered for ED estimation only if: (i) recycling ratio was within 1±0.1, (ii) ED error was less than 20%, (iii) test dose error was less than 10%, and (iv) recuperation was below 5% of the natural. For samples K16 and K17 (fluvial sand trapped above the T3 strath surface), the feldspar contamination was negligible. Therefore, the OSL SAR protocol was tried with test doses of 50 Gy, 100 Gy, and 150 Gy, respectively. Samples K16 and K17 returned highly scattered equivalent dose (De) estimates (over-dispersion > 30%) (cf. Table 2), and thus, both of them have been interpreted by the minimum age model (Bailey and Arnold, 2006). Sample K18 (from the silty clay layer found above the T1 strath surface in the wind gap of Maru River) (cf. Fig.9b) was saturated, and

hence, we also provided the minimum age estimate for the same. The sample was exhausted after we performed OSL measurements. Therefore, we couldn't proceed towards feldspar dating with sample K18.

OSL dating for the three samples procured from the fluvio-glacial sediments showed saturation; therefore, we tried for IRSL (Infra-red stimulated luminescence) dating of feldspar for those three samples (K07-K09) using standard post infrared (pIR-IR) protocol (Buylaert et al., 2013), in which, the preheat temperature was 320°C for 60s. The samples were first stimulated at 50°C with IR diodes for 100s followed by IR stimulation at 290°C, and a violet-blue luminescence emission (395 ± 50 nm) was detected by PMT through the combination of optical filters, Corning 7-59 (4 mm) and BG-39 (2 mm). However, the samples showed significant saturation, possibly due to improper bleaching of the Post-IR IRSL signal. The IRSL signal is not saturated, suggesting it to be better bleached. We encountered a significant IRSL signal while testing the luminescence of hand-picked individual quartz grains, indicating a presence of feldspar inclusion within the quartz. We tried leaching with 40% HF for three times, which exhausted most of the separated quartz sample. Hence, we had to proceed with standard IR protocol (Preusser, F., 2003) using K-feldspar. The initial test dose for the samples was set for 150 Gy, and the rest of the runs were set for 375 Gy and 750 Gy, respectively (Fig.5). Fading correction tests were done for two samples (K07 and K09), and the fading correction factors have been calculated using conventional methods after Huntley and Lamothe (2001). The over-dispersion values are less than 30% (cf. Table 2). Hence, Central Age Model (CAM) has been used for estimation of equivalent dose (De) (Bailey and Arnold, 2006) instead of RMM-based De estimation as prescribed by Chauhan and Singhvi (2011), useful for samples having higher over-dispersion.

The dose rate was estimated using online software DRAC (Durcan et al., 2015) from the data of Uranium (U), Thorium (Th) and Potassium (K) measured using ICP-MS and XRF (Table

2) in IISER Kolkata. The estimation of moisture content was done by using the fractional difference between the saturated vs. unsaturated sample weight. Shine curve, dose growth curve, and radial plots for De estimation obtained from the analysis of three representative samples: K07 (IRSL), K11 (OSL D-SAR) and K17 (OSL SAR) are shown in Supplementary Fig.B5.

4. Results

4.1.Field observations and measurements

The Chenab River has deeply incised the KW (Fig. 3a). The LH metasediments exposed within the KW are mainly composed of Rampur Quartzites (Fig.2b,2d) and phyllites with occasional schists in between. (Steck, 2003; Gavillot et al., 2018). The LHD has been suggested to be an asymmetric antiformal stack with a steeper western flank (dip: 70°/west) (Fig.8a). The KW is surrounded by rock units related to the Higher Himalayan high-grade metasedimentary sequence (HHCS), mainly garnet-bearing mica schists and gneisses (Fig.2a). Higher Himalayan rocks close to the western edge of the KW form a syncline with a southwest-verging MCT at its' base. The KT, southern structural boundary of the window margin, accommodating the differential exhumation between the window and the surroundings – and it is expressed as highly deformed sub-vertical shear bands (Fig.2b).

Along the traverse of the Chenab River through the window and further downstream, two prominent stretches of ~20 and ~25-30 km length have been identified where the channel gradients are high (Fig.7c), and we observed a sequence of rapids (FFig.3a,3e). These steep segments are also characterized by a very narrow channel width (< 30m) (Fig. 7b). These two steepened segments define knickzone rather than a single knickpoint. We refer to the knickzone at the core of the window as K1 and the one downstream from the KW as K2 (Fig.6, 7). The knickzones are hosted over bedrock gorges, and field evidence confirms that

none of them (downstream from the eastern edge of the KW) are related to damming by landslides or other mass movements. The east margin of the KW is characterized by a broad 'U-shaped' valley filled with thick sand layers and coarser fluvioglacial sediments. The River incises through this Late Pleistocene fill at present (*F*Fig.3a).

The rock strength data taken along the Chenab River shows large variations across different morphotectonic segments (Fig.7e). Within the KW, Lesser Himalayan phyllites and schists have low R values (30-35); however, the low-strength schists and phyllites are sparsely present and therefore, they were ignored while plotting the regional rock strength values in Fig.7e. The dominant Rampur quartzites in the KW, as well as the granitic intrusives in the eastern part of the KW, shows very high R values of 51±4 and 58±2, respectively (Fig.7e). Compared to the high R values in the KW, the Higher Himalayan migmatites near the KT (western margin of the KW) show moderate strength (R: 49±5)whereas, the HHCS units show lower strength (R: 39±3). The rock strength increases (R: 44±2) within the Haimanta Formation until it reaches the MCT shear zone. The R-value in the frontal Lesser Himalaya is moderate (R: 41±2).

*F*R

FF

4.2. Results from morphometric analysis

4.2.1. Steep stream segments and associated knickpoints

The longitudinal stream profile along the Chenab River does not portray a typical adjusted concave-up profile across the Himalaya (Fig. 6,7a). We observed breaks in slope and concavity at least at six occasions within a ~170 km traverse upstream from the MBT (point A, cf. Fig.1a) (Fig.7a). These breaks are defined as knickpoints or knickzones, depending on their type characteristics. The slope breaks represent the upstream reaches of the steep stream segments. The basinwide steepness indices span from ~30- >550 $m^{0.9}$ across the study area

(Fig. 5d). We assigned a threshold value of k_{sn}>550 for the steepest watersheds/ stream segments. Along the traverse, the major knickpoints are L1 (~1770m), K1 (~1700m), K2 (~1150m), K3 (~950m), L2 (~750m) and D1 (~700m) respectively (Fig.7a).

Already Nennewitz et al. (2018) had proposed a high basin-averaged k_{sn} value of > 300 in the KW. Here in this study, we worked with a much-detailed DEM for stream-specific k_{sn} allocation (FFig.5d), as well as a basinwide steepness calculation with smaller watersheds. Our results corroborate with the earlier findings, but predicts the zone of interest in greater detail. It is important to note that by setting a higher tolerance level in the 'knickpointfinder' tool in Topotoolbox, we have managed to remove most of the DEM artifacts from consideration (Schwanghart and Scherler, 2014).

4.2.2. Channel width and valley morphology

The channel width of the Chenab river is on average low (30-60m) within the core of the KW (Fig. 7b), and the low channel width continues till the Chenab River flows N-S along the western margin of the KW. However, there are a few exceptions; upstream from the knickpoint L1 in the Padder valley (in which the town of Padder is located), the channel widens (width ~80-100m), and the channel gradient is low (Fig. 3a,7b,7c). The second instance of a broader channel is seen upstream from knickpoint K2, where there is a reservoir for the Dul-Hasti dam (Fig.7b). Downstream from K2 within the Higher Himalaya, the channel width ranges from 50-70 m. However, towards the lower stretches of the N-S traverse, the width is even lower (16-52m). The river width increases to 100-200m as Chenab River takes a westward path after that. The river width increases beyond 300m until it leaves the crystalline rocks in the hanging wall of the MCT and enters the Lesser Himalaya in the hanging wall of the MBT across the Baglihar dam. Within the frontal LH, the channel width is again lowered (50-80 m).

4.2.3. RR*Changes in specific stream power (SSP)*

Discharge-normalized SSP data calculated from the upstream stretches and the knickzones, K1 and K2, show a significant increase in SSP within the steep knickzones. The rise in SSP from upstream to the knickzones K1 and K2 is 4.44 and 5.02 times, respectively (Table 1). Such a high increase in SSP is aided by the steepening of channel gradient and narrowing of the channel.

4.3. Luminescence chronology

The results for the luminescence chronology experiment are listed in Table 2 and the shine curve, dose growth curve and De estimation plots for different samples are provided in the supplementary Fig.S3. Sample K07, K08 and K09 yield IRSL ages of 104.5±5.9 ky, 114.4±6.3 ky, and 119.2±6.8 ky, respectively. Fading corrections done for samples K07 and K09 yield the correction factors (g%) of 0.89 and 1.11, respectively. The sample K08 has not been treated for fading correction. Still, for easier understanding, we have assumed a constant sedimentation rate between the samples K07 and K09 and extrapolated the 'fading-corrected' age for K08. The oldest sample K09 (132±7 ky) (fading-corrected IRSL age) is succeeded by samples K08 (126±6 ky) and K07 (113±6 ky), respectively (Fig.4c). The initial IRSL ages (before fading-correction), therefore, may be regarded as a minimum age estimate for the fluvioglacial sediment sequence. The finer fraction of the hillslope debris overlying the fluvioglacial deposits yields OSL ages of 81.1±4.6 ky (K02) and 85±5 ky (K11) (Fig.4d, 4e). OSL samples taken from sparsely-preserved sediment layers above the T3 strath surface show heterogeneous bleaching, and hence we provide a minimum age of 22.8±2.1 ky (sample K16) and 20.5±1.0 ky (sample K17). One sample taken above the T1 strath level is saturated and shows a minimum age of 52.1±2.8 ky (sample K18) (Table 2).

5. Discussions

Morphometric parameters are widely used as indicators of active tectonics and transient topography (Hack, 1973; Kirby and Whipple, 2012; Seeber and Gornitz,1983). Many studies have used morphometry as a proxy for understanding the spatial distribution of active deformation across specific segments of the Himalayan front (Malik and Mohanty, 2007; van der Beek et al., 2016; Nennewitz et al., 2018; Kaushal et al., 2017). More importantly, some studies have integrated morphometric analysis with rigorous chronological constraints to assess the spatial and temporal variability in deformation within the Sub-Himalaya (Lave and Avouac, 2000; Thakur et al., 2014; Vassalo et al., 2015; Dey et al., 2016; Srivastava et al., 2018). In this section, we discuss how we combined terrain morphometry and Quaternary dating of sediments to evaluate ongoing deformation in the interior of the NW Himalaya.

Apatite fission-track cooling ages at the center of the LH duplex and along the western margin of the KW are younger (~2-3 Ma) as compared to the surrounding Higher Himalaya. Young AFT cooling ages have been interpreted as the result of rapid exhumation of the LH duplex over million-year timescale (Kumar et al., 1995; Gavillot et al., 2018). However, to date, we lack any estimate of deformation on the 10^3-10^5-year timescale. Thus, we have come up with a detailed morphometric analysis of the terrain and structural data to decipher the spatial distribution of faulting and fault patterns. With additional chronological constraints from late Quaternary sedimentary deposits, we predict rapid fluvial bedrock incision in the Himalayan interiors.

5.1. Knickpoints and their genesis

Already Seeber and Gornitz (1983) showed that the Chenab River is characterized by a zone of steep channel gradient in the vicinity of the KW. Thiede and Ehlers (2013) demonstrated a strong correlation between steeped longitudinal river profiles and young thermochronological cooling ages, suggesting focused rock uplift and rapid Quaternary exhumation along many

major rivers draining the southern Himalayan front. Although, it is still an open debate whether uplift and growth of the LHD are triggered solely by slip over the crustal ramp of the MHT or additional out-of-sequence surface-breaking faults are augmenting it (Avouac et al., 2001; Herman et al., 2010; Elliot et al., 2016; Whipple et at., 2016).

The longitudinal profile of the lower Chenab traverse (below ~2000 m above MSL) is punctuated by two prominent stretches of knickpoint zones (Fig.7a). Below we will discuss the potential cause of formation of those major knickpoints in the context of detailed field observation, of existing field-collected structural and lithological data, geomorphic features, rock strength, and channel width information (*Fig.3b*).

5.1.1. Lithologically-controlled knickpoints

The Himalayan traverse of the Chenab River is characterized by large variations in substrate lithology and rock strength (Fig.7a). These variations have inflicted their 'marks' on the river profile. An instance of soft-to-hard substrate transition happens across the knickpoint L1, lying downstream from the Padder valley, at the eastern edge of the KW (Fig.3a, 7). Across L1, the River enters the LH bedrock gorge (R value> 55) after exiting the Padder valley filled with unconsolidated fluvioglacial sediments (Fig.3a). A similar soft-to-hard substrate transition is observed upstream from the MCT shear zone. The corresponding knickpoint L2 represents a change in lithological formation from the sheared and deformed Higher Himalayan crystalline (R value~35-40) to deep-seated Haimantas (R value~40-50) (Fig.7a). There is no field evidence, such as fault splays or ramps, in support of L2 to be a structurally-controlled one.

5.1.2. Tectonically-controlled knickpoints

Compiling previously-published data on regional tectonogeomorphic attributes (Gavillot et al., 2018) with detailed field documentation of structural styles and tectonic features, we have deciphered the role of rock-uplift and variable structural styles in the interiors of the NW

Himalaya. We have found at least two instances where knickpoints are not related to change in substrate, nor are they artificially altered.

The knickzone K1 (~1700 m above MSL) represents the upstream reach of a steepened stream segment of run-length ~18-20 km. The upstream and downstream side of K1 is characterized by a change in the orientation (dip angle) of the foliation of the LH bedrock (Fig.2f, 2g). Across K1, the dip amount of the foliation planes change from ~25-30° to ~60-65° (both cases dip towards east). K1 also reflects a narrowing of the channel width (Fig. 7b) and an increase in channel gradient (Fig.7c) and ksn value (Fig.7d). Near the end of the steep segment, we observed intensely-deformed (folded and fractured) LH rocks (Fig.2d, 2e). We explain this as evidence of faulting within the LH duplex and the steep stream segment represents the ramp of the fault or fault zone between two duplex nappes (Fig.8d). K1, therefore reflects the transition from flat to ramp of the existing structure soled to the basal decollement. The steep segment represents a drop of ~420m of the Chenab River across a run-length of ~20 km (Fig.8c). In addition to this, we may comment that the schists and phyllites within the Lesser Himalayan sequence probably act as the basal planes of the thrust nappes.

On the other hand, the other knickpoint K2 nearly coincides with the exposure of the KT (Fig.7a). K2 cannot be a lithologically-controlled knickpoint as it reflects no significant change in substrate hardness, at least not a soft-to-hard substrate transition. LH quartzites (R value: 51±4) and HH migmatites (R value: 49±5) have similar rock hardness (cf. Fig.7e). However, in the longitudinal profile, K2 does not represent a sharp slope break because the downstream segment runs parallel for ~25-30 km and not perpendicular to the orientation of all major structures of the orogen, including the KT. Therefore, we performed an orthogonal projection of the E-W trending traverses of the Chenab River and tried to estimate an orogen-perpendicular drop of the Chenab across K2 (Fig. 8d). The truncated profile across K2 shows

a drop of ~230m of the channel across an orogen-perpendicular run-length of ~5 km. The orogen-parallel stretch of the River exhibits narrow channel width (<30-35m) through a moderately hard HH bedrock (R-value: 35-45). The tributaries within this stretch form significant knickpoint at the confluence with the trunk stream (Fig. 3f). These pieces of evidence hint towards a rapid uplift of the HH rocks along the western margin of the KT and are possibly related to the presence of another crustal ramp emerging from the MHT (Fig.8b). Both the knickzones, K1 and K2 portray transiently-high specific stream power values (Table 1), which we relate to the fact that the knickzones are undergoing much rapid fluvial incision than the rest of the study area. If we consider the fluvial incision as a proxy of relative uplift (assuming a steady-state), we may well say that the knickzones define the spatial extent of the areas undergoing differential uplift caused by movement on the fault ramps.

5.1.3. Knickpoint marking epigenetic gorge

Epigenetic gorges are common geomorphic features in the high-mountain landscape (Ouimet et al., 2008). Epigenetic gorges form when channels of a drainage system are buried by sediment aggradation and during subsequent re-incision, a new river channel is incised. The N-S traverse of the Chenab River is largely affected by hillslope sediment flux from the steep eastern flank. The knickpoint K3 situated near the village of Janwas, mark one such instance of epigenetic gorge where the paleo-valley has been filled initially by fluvioglacial sediments and the channel abandonment was caused by hillslope debris flow ~80 ky (Fig.4b, 4c).

5.2. Sediment aggradation in the Chenab valley

The luminescence chronology of the transiently-stored sediments in the Chenab valley point towards protracted sediment aggradation since the onset of the last glacial-interglacial cycle till ~80 ky. Fluvioglacial outwash sediments range from ~110-130 ky, whereas the hillslope debris range from ~90 to ~80 ky (cf. Fig.4). The obtained chronology of the sediment deposits match well with the relative stratigraphic order of the sedimentary units, and

therefore, we believe the obtained ages are reliable. The deeply-incised fluvial network as we observe today require net fluvial incision and formation of bedrock strath surfaces sometime after ~80 ky before present.

5.3. Drainage re-organization and strath terrace formation along Chenab River

Hillslope debris flow characterized by white quartzite blocks of different sizes and shapes can only originate from the high-relief frontal horses of the Lesser Himalayan Duplex exposed in the eastern flanks of the valley. These hillslope debris overlies the fluvioglacial sediments stored beneath the Kishtwar surface (Fig.9a, 9c). We argue that the hillslope debris flow intervened in the paleo-drainage of the Chenab River, which might have been flowing through an easterly path than now (Fig.9). The Maru River, coming from the north-western corner of our study area, was also joining the Chenab River at a different location (Fig.9). Our argument is supported by field observation of the thick silt-clay layer in the proposed paleo-valley of the Maru River (Fig.9a, 9c). OSL sample (K18) from the silt-clay layer is saturated and hence only provides the minimum age of 52±3 ky. We suggest that the hillslope sediment flux has ceased the flow of the Chenab River and also propagated through the wind-gap of the Maru River. The decline in depositional energy has resulted in a reduction of grain-size. Post-hillslope debris flow episode, the Chenab River also diverted to a new path. The new course of the Chenab River upstream from the confluence with the Maru River is defined by a very narrow channel flowing through the Higher Himalayan bedrock gorge (Fig.9). Downstream from the confluence, we identified at least three levels of strath terraces lying at heights of ~280-290m (T1), ~170m (T2), and ~120m (T3), respectively (Fig.4g, 10a). Our field observation suggests that the formation of the straths is at least ~52 ky-old. The luminescence chronology samples in this study belong to the ~150-170m-thick soft sediments that are stored stratigraphically-up from the T1 strath level. Our

field observations and chronological estimates suggest that the renewed path of the Chenab River must have been formed post the hillslope debris flow ~80-90 ky but before 52 ky.

5. 4. Rapid bedrock incision along Chenab River

Considering the rate of excavation of softer sediments to be at least an order of magnitude higher than the rate of bedrock incision (Ouimet et al., 2008; Kothyari and Juyal, 2013), we calculated the minimum bedrock incision rate using the height of the T1 strath (~280±5 m) and the average age of the sediments from the Hillslope debris flow deposit. It yields a minimum bedrock incision rate of ~3.1-3.5 mm/y over the last 80-90 ky. Considering the saturated OSL sample from the paleo-valley, we estimated the maximum bedrock incision since 52 ky to be 5.1-5.5 mm/y. Similarly, using the minimum age estimate of the T3 terrace abandonment, we deduce a maximum bedrock incision rate of ~5.7-6.1 mm/y since ~21 ky (Fig.10b).

Many studies have used dated strath surfaces to quantify rock uplift rates in the Himalaya (Wesnousky et al., 1999; Lave and Avouac, 2000; Mukul et al., 2007; Thakur et al., 2014). Assuming the channel hypsometry to be constant during the incision period, we may infer the minimum fluvial incision reflects regional rock uplift caused by movement of rocks over the ramp of the MHT at a rate of ~3.1-3.5 mm/y. This minimum uplift rate estimate is in agreement with long-term exhumation rates of 3.2-3.6 mm/y deduced from the KW (Gavillot et al., 2018). The inferred uplift rate can be translated to a shortening rate by using a simple trigonometric function. Our field findings suggest that the larger ramp on the MHT (MCR-1) have an average near-surface dip of ~60˚. Considering a similar geometry for MCR-2, we obtained a minimum shortening rate of 1.8-2.0 mm/y. On the other hand, considering the minimum ages of T3 terrace abandonment, we obtained maximum uplift rates ~5.5-6.0 mm/y, which would translate into a shortening rate of ~3.2-3.5 mm/y since ~21 ky.

5.5. Our findings in context with the previously-published data

The young AFT-cooling ages by the pioneering work of Kumar et al., (1995) showcased a rapid exhumation of the KW (AFT ages: ~1-3 My) compared to the surroundings (AFT age: 6-12 My). The exhumation rates proposed by Gavillot et al. (2018) is based on using a geothermal gradient of 35-40˚C/km in Dodson's equation assuming a 1-D model (Dodson, 1973). Unfortunately, a proper thermal modeling of the region is lacking, therefore, regional correlation with the proposed cooling ages and exhumation rates has large uncertainties. However, lateral similarities of the regional topography and similar thermochronologic age patterns obtained along the Sutlej area, Beas and Dhauladhar Range (Thiede et al., 2017; Thiede et al., 2009; Stübner et al., 2018) have yielded exhumation rates in the range of 2-3 mm/y. Long-term exhumation rates from the NW Himalaya agree well with the findings of Nennewitz et al. (2018). Their study recognized a strong correlation between the young thermochron ages with high basinwide k_{sn} values suggesting high uplift rates over intermediate to longer timescales. Therefore, the proposed range of long-term exhumation rates of 3.2-3.6 mm/y determined by Gavillot et al. (2018) agree with the regional data pattern. Although the geomorphic implications on landscape evolution are valid for shorter timescales than the low-T thermochron studies, we must comment that our field observations and analysis support a protracted growth of the LH duplex exposed within the boundaries of the KW. Unless there has been a recent growth of the duplex, the geomorphic signatures would have been subdued. Young low-T thermochron ages (Kumar et al., 1995) had been sampled from the steepened stream reaches, where the SSP is high. Interestingly, exhumation rates obtained from the steepened stretches is ~ten times more than that of the Higher Himalaya in the hanging wall of the duplex. Our estimates of SSP also reflect an increase by ~five times within the steepened stretches.

Deeply-incised channel morphology, steep channel gradients marked by knickpoints at the upstream reaches in and around the KW could be explained by the presence of at least two

orogen-parallel mid-crustal ramps on the MHT (Fig.8b). The existence of two mid-crustal ramps have already been suggested by Gavillot et al., (2018) (Fig.S2). However, the internal structural orientation of the LH duplex published by Gavillot et al., (2018) (Fig. S2) differ considerably from our field observations (Fig.2, Fig.8b). Our morphometric analysis and field observation indicate pronounced deformation at the core of the KW suggesting that this is related to active faulting or internal folding at the base of the steepened stretch of K1*F*. The ramp of the fault-zone mentioned above triggers the rapid exhumation of the hanging wall. It causes high relief, steep channel gradients and higher basinwide steepness indices over the ramp (Fig.7). Similar ramps have been proposed on the MBT beneath the Dhauladhar Range (Thiede et al., 2017) and in the east of the NW Himalaya (Caldwell et al., 2013; Mahesh et al., 2015; Stübner et al., 2018; Yadav et al., 2019). We don't have any direct field evidence of surface-breaking faults, which could be linked to the MCR-2. However, a rapid fluvial incision along the western margin of KW and an increase in morphometric parameter values (k_{sn}, channel gradient, topographic relief, etc.) probably justify the existence of MCR-2.

Our findings from the Kishtwar region of the NW Himalaya establish the importance of morphometric parameters in the assessment of intermediate timescales of 10^4-10^6 years. We can resolve variations in the tectonic imprint on landscape evolution by analyzing the topography with high-resolution DEM. Earlier studies used to process larger areas, but the resolution of those data and findings is coarse (Nennewitz et al., 2018).

Models explaining the spatial distribution of the high uplift zone in the interiors of the Himalaya favor the existence of a mid-crustal ramp, which has variable dimension, geometry, and distance from the mountain front along-strike of the Himalayan orogeny (Robert et al., 2009). Our data support the idea of mid-crustal ramps beneath the Higher Himalayan domain (Nennewitz et al., 2018) and we predict that the seismic hypocenters are clustered in the vicinity of the ramp of MHT and within the LHD and are linked to the ongoing growth of the

duplex. Our results verify the previously-suggested models that there exist two orogen-parallel small ramps beneath the Kishtwar Window instead of one (Gavillot et al., 2018). However, we must also comment that the previous model, as well as the balanced cross-section, lack detailing and the thermochron data (Kumar et al., 1995) is sparse. Therefore, field observation and the detailed morphometric analysis using high-resolution DEM help to measure the spatial extent of deformation. We can resolve the high-relief Kishtwar Window and the surroundings into two major steep orogen-parallel belts/ zones (Fig. 4a). While the larger one is an active high-angle fault-ramp emerging from the MHT and causing sustained uplift in the core of the duplex, the smaller one lies along the western margin of the KW. We suggest that this has two major implications. One, we have evidence for ongoing internal deformation of duplex, and that entire window is still tectonically-active – and therefore this could be a potential source future seismic activity. Our finding contradicts with the existence of a single major ramp in the interiors of the Himalaya, as described from other sectors of the Himalaya (Gahalaut and Kalpna, 2001; Elliot et al., 2016; Thiede et al., 2017).

Nennewitz et al., (2018) have proposed that the million-year-timescale shortening achieved in the interior of the Himalaya near the Sutlej-Beas area in the eastern Himachal Pradesh is caused by accentuated rock uplift over a ramp at a mid-crustal depth of ~ 8-25 km on the MHT. In contrast, studies from the Dhauladhar Range in the north-western Himalaya hints the presence of deep-seated crustal ramp on the MBT and yielded a shortening rate of 3±0.5 mm/y across the MBT over the last 8 My and absence of mid-crustal ramp (Deeken et al., 2011; Thiede et al., 2017). The work by Gavillot et al. (2018) favors the existence of at least two mid-crustal ramps beneath the KW (Supplementary Fig.S2). Their suggestion is in agreement with very young AFT cooling ages (1-3 Ma) (Kumar et al., 1995) in the window (Fig.1a) and the findings of this study. These studies altogether point out the along-strike variation in the location of the rapidly-uplifting crustal ramp with respect to the southern

Himalayan front. The crustal ramp in the nearby Kangra recess is located beneath the Dhauladhar Range at the main Himalayan front, whereas, in the Himalayan transects situated towards the east and west of Kangra recess, the ramps are located ~100km inside from the MBT. Topographic relief and basinwide mean k_{sn} distribution (Fig.5) hint towards the existence of a lateral ramp in between the Kangra and the Jammu-Kashmir Himalayan transects. However, at this moment, we have no conclusive data in support of this claim.

6. Conclusions

Our field observation and the characteristics of terrain morphology match well with the spatial pattern of previously-published thermochronological data and unanimously indicate that the Kishtwar Window is undergoing active and focused uplift and exhumation at present, during intermediate timescales, and in geological past since at least the late Miocene. By compiling our new results and published records, we favor the following conclusions:

1. The Chenab maintains an over-steepened bedrock channel and a low channel width irrespective of any lithological variations across the KW and beyond, suggesting ongoing rapid fluvial incision.
2. Our field observations, morphometric analysis, and rock strength measurements document that at least two of these major knickzones on the trunk stream are non-lithologic and preferably can be related to differential uplift of the rock units. The incision potential in the steepened stretches ~4-5 times higher than the surroundings.
3. The differential uplift is most-likely related to variations in the geometry of the basal decollement and out-of-sequence surface-breaking fault/s. Our results favor the presence of at least two mid-crustal ramps beneath the

Kishtwar Window and the surroundings, as compared to a single crustal ramp proposed from interiors of the nearby sectors of the NW Himalaya.

4. The larger of the proposed crustal ramps emerge as an active high-angle ramp at the core of the Lesser Himalayan Duplex and cause sustained faulting and uplift of the hanging wall.
5. Luminescence chronology of the transiently-stored sediments along the Chenab River suggests that the valley had been overfilled with deposits of fluvioglacial origin as well as with hillslope debris flow. Massive sediment aggradation during ~130-80 ky led to drainage re-organization and bedrock incision, leaving behind a set of strath surfaces.
6. The late Quaternary bedrock incision rates on the mid-crustal ramp beneath the western margin of the KW are high 3.1-3.6 mm/y. We argue that this rapid fluvial incision can potentially be linked to the accommodation of crustal shortening along a mid-crustal ramp of the basal decollement of the Himalaya. Our results indicate a minimum shortening rate of ~1.8-2.1 mm/y being accommodated along the N-S traverse of the Chenab River.

Our study refutes the long-standing hypothesis of nearly 100% accommodation of crustal shortening within the Sub-Himalaya since late Pleistocene-Holocene time and provides new insights on the structural styles and ongoing out-of-sequence deformation in the Himalayan interiors.

Appendix

Additional maps, figures on morphometric analysis and luminescence dating are listed in Appendix A. Data of rock strength measurements provided in Table C1.

Code availability

Authors used open-source codes of Topotoolbox and Topographic Analysis Kit Toolbox for this study.

Data availability

Field data are already provided in Appendix 1. Additional data on luminescence dating can be provided on request.

Sample availability

Samples used for luminescence dating are already mostly-destroyed, therefore it is beyond sharing.

Author contribution

S.Dey, the first author, this work and completed the fieldwork, sample processing, measurements and writing of this manuscript. R. Thiede helped in fieldwork, discussion and writing of this manuscript. A. Biswas performed the initial morphometric analysis. N.Chauhan helped in measurement of luminescence signal and assessment of the data. P.Chakravarti performed the channel width calculations and compiled the rock strength measurements. V. Jain helped in discussion and writing of the manuscript.

Competing interests

The authors declare that they have no conflict of interest.

Acknowledgments

This study is funded by the DST INSPIRE faculty fellowship program by the Department of Science and Technology, India (grant #DST/INSPIRE/04/2017/003278), and IIT Gandhinagar post-doctoral research fund (IP/IITGN/ES/SD/201718-01). Thiede is supported by German Science Foundation (grant # DFG TH 1317-8 and 9). We thank M.K.Jaiswal and

M.Rawat for providing the XRF elemental analysis. We thank Shambhu Das, Avi Das, Niklas Schaaf, Akashsingh Rajput and Chamel Singh for their assistance during fieldwork. We also thank Soumyajit Mukherjee, Rahul Kaushal and Shantamoy Guha for scientific inputs and comments on this manuscript.

References

Aitken, M. J. (1992). Optical dating. Quaternary Science Reviews, 11(1-2), 127-131.

Bagnold, R. A. (1966). An approach to the sediment transport problem from general physics. US government printing office.

Bailey, R. M., & Arnold, L. J. (2006). Statistical modelling of single grain quartz De distributions and an assessment of procedures for estimating burial dose. *Quaternary Science Reviews*, *25*(19-20), 2475-2502.

Bhatia, T. R., & Bhatia, S. K. (1973). Sedimentology of the slate belt of Ramban-Banihal area, Kashmir Himalaya. Himalayan Geology, 3, 116-134.

Bollinger, L., Henry, P., & Avouac, J. P. (2006). Mountain building in the Nepal Himalaya: Thermal and kinematic model. *Earth and Planetary Science Letters*, *244*(1-2), 58-71.

Bookhagen, B., & Burbank, D. W. (2006). Topography, relief, and TRMM-derived rainfall variations along the Himalaya. Geophysical Research Letters, 33(8).

Brozovic, N., & Burbank, D. W. (2000). Dynamic fluvial systems and gravel progradation in the Himalayan foreland. GSA Bulletin, 112(3), 394-412.

Burbank, D. W., Leland, J., Fielding, E., Anderson, R. S., Brozovic, N., Reid, M. R., & Duncan, C. (1996). Bedrock incision, rock uplift and threshold hillslopes in the north-western Himalayas. *Nature*, *379*(6565), 505.

Burgess, W. P., Yin, A., Dubey, C. S., Shen, Z. K., &Kelty, T. K. (2012). Holocene shortening across the Main Frontal Thrust zone in the eastern Himalaya. Earth and Planetary Science Letters, 357, 152-167.

Buylaert, J.P., Murray, A.S., Gebhardt, A.C., Sohbati, R., Ohlendorf, C., Thiel, C., Wastegård, S., Zolitschka, B. and Team, T.P.S., 2013. Luminescence dating of the PASADO core 5022-1D from Laguna Potrok Aike (Argentina) using IRSL signals from feldspar. *Quaternary Science Reviews*, *71*, pp.70-80.

Caldwell, W. B., Klemperer, S. L., Lawrence, J. F., and Rai, S. S., 2013, Characterizing the Main Himalayan Thrust in the Garhwal Himalaya, India with receiver function CCP stacking: Earth and Planetary Science Letters, v. 367, p. 15-27.

Chauhan, N., & Singhvi, A. (2011). Distribution in SAR palaeodoses due to spatial heterogeniety of natural beta dose. *Geochronometria*, *38*(3), 190-198.

Cunningham, A. C., & Wallinga, J. (2012). Realizing the potential of fluvial archives using robust OSL chronologies. *Quaternary Geochronology*, *12*, 98-106.

DeCelles, P. G., Robinson, D. M., Quade, J., Ojha, T. P., Garzione, C. N., Copeland, P., and Upreti, B. N., 2001, Stratigraphy, structure, and tectonic evolution of the Himalayan fold-thrust belt in western Nepal: Tectonics, v. 20, no. 4, p. 487-509.

Deeken, A., Thiede, R. C., Sobel, E. R., Hourigan, J. K., & Strecker, M. R. (2011). Exhumational variability within the Himalaya of northwest India. Earth Planetry Science Letters, 305(1-2), 103–114. https://doi.org/10.1016/j.epsl.2011.02.045

Dey, S., Kaushal, R. K., & Jain, V. (2019). Spatiotemporal variability of neotectonic activity along the Southern Himalayan front: A geomorphic perspective. Journal of Geodynamics, 129, 237-246.

Dey, S., Thiede, R. C., Schildgen, T. F., Wittmann, H., Bookhagen, B., Scherler, D., & Strecker, M. R. (2016). Holocene internal shortening within the northwest Sub-Himalaya: Out-of-sequence faulting of the Jwalamukhi Thrust, India. Tectonics, 35(11), 2677-2697.

DiPietro, J. A., & Pogue, K. R. (2004). Tectonostratigraphic subdivisions of the Himalaya: A view from the west. Tectonics, 23(5).

Dodson, M. H. (1973). Closure temperature in cooling geochronological and petrological systems. Contributions to Mineralogy and Petrology, 40(3), 259-274.

Elliott, J. R., Jolivet, R., González, P. J., Avouac, J. P., Hollingsworth, J., Searle, M. P., & Stevens, V. L. (2016). Himalayan megathrust geometry and relation to topography revealed by the Gorkha earthquake. *Nature Geoscience*, *9*(2), 174.

Eugster, P., Scherler, D., Thiede, R. C., Codilean, A. T., and Strecker, M. R., (2016). Rapid Last Glacial Maximum deglaciation in the Indian Himalaya coeval with midlatitude glaciers: New insights from 10Be-dating of ice-polished bedrock surfaces in the Chandra Valley, NW Himalaya: Geophysical Research Letters, v. 43, no. 4, p. 1589-1597.

Finnegan, N. J., Roe, G., Montgomery, D. R., &Hallet, B. (2005). Controls on the channel width of rivers: Implications for modeling fluvial incision of bedrock. *Geology*, *33*(3), 229-232.

Flint, J. J. (1974). Stream gradient as a function of order, magnitude, and discharge. Water Resources Research, 10(5), 969-973.

Forte, A.M. and Whipple, K.X. (2019). The Topographic Analysis Toolkit (TAK) for Topotoolbox. Earth Surface Dynamics, 7, 87-95.

Gahalaut, V. K., & Kalpna. (2001). Himalayan mid-crustal ramp. *Current Science*, 1641-1646.

Gavillot, Y. G. (2014). Active tectonics of the Kashmir Himalaya (NW India) and earthquake potential on folds, out-of-sequence thrusts, and duplexes.

Gavillot, Y., Meigs, A. J., Sousa, F. J., Stockli, D., Yule, D., & Malik, M. (2018). Late Cenozoic Foreland-to-Hinterland Low-Temperature Exhumation History of the Kashmir Himalaya. Tectonics.

Gavillot, Y., Meigs, A., Yule, Y., Heermance, R., Rittenour, T., Madugo, C., & Malik, M. (2016). Shortening rate and Holocene surface rupture on the Riasi fault system in the Kashmir Himalaya: Active thrusting within the Northwest Himalayan orogenic wedge. Geological Society of America Bulletin, 128(7-8), 1070–1094. https://doi.org/10.1130/B31281.1

Hack, J. T. (1973). Stream-profile analysis and stream-gradient index. Journal of Research of the us Geological Survey, 1(4), 421-429.

Harvey, J. E., Burbank, D. W., & Bookhagen, B. (2015). Along-strike changes in Himalayan thrust geometry: Topographic and tectonic discontinuities in western Nepal. Lithosphere, 7(5), 511-518.

Herman, F., Copeland, P., Avouac, J.P., Bollinger, L., Mahéo, G., Le Fort, P., Rai, S., Foster, D., Pêcher, A., Stüwe, K. and Henry, P., 2010. Exhumation, crustal deformation, and thermal structure of the Nepal Himalaya derived from the inversion of thermochronological and

thermobarometric data and modeling of the topography. *Journal of Geophysical Research: Solid Earth*, *115*(B6).

Hirschmiller, J., Grujic, D., Bookhagen, B., Coutand, I., Huyghe, P., Mugnier, J.-L., and Ojha, T., 2014, What controls the growth of the Himalayan foreland fold-and-thrust belt?: Geology, v. 42, no. 3, p. 247-250.

Huntley, D. J., & Lamothe, M. (2001). Ubiquity of anomalous fading in K-feldspars and the measurement and correction for it in optical dating. *Canadian Journal of Earth Sciences*, *38*(7), 1093-1106.

Kaushal, R. K., Singh, V., Mukul, M., & Jain, V. (2017). Identification of deformation variability and active structures using geomorphic markers in the Nahan salient, NW Himalaya, India. *Quaternary International*, *462*, 194-210.

Kothyari, G. C., & Juyal, N. (2013). Implications of fossil valleys and associated epigenetic gorges in parts of Central Himalaya. *Current Science*, 383-388.

Kumar, A., Lal, N., Jain, A. K., &Sorkhabi, R. B. (1995). Late Cenozoic–Quaternary thermo-tectonic history of Higher Himalayan Crystalline (HHC) in Kishtwar–Padar–Zanskar region, NW Himalaya: Evidence from fission-track ages. Journal of the Geological Society of India, 45(4), 375–391.

Kundu, B., Yadav, R. K., Bali, B. S., Chowdhury, S., &Gahalaut, V. K. (2014). Oblique convergence and slip partitioning in the NW Himalaya: implications from GPS measurements. Tectonics, 33(10), 2013-2024.

Lavé, J., & Avouac, J. P. (2000). Active folding of fluvial terraces across the Siwaliks Hills, Himalayas of central Nepal. Journal of Geophysical Research: Solid Earth, 105(B3), 5735-5770.

Lavé, J., & Avouac, J. P. (2001). Fluvial incision and tectonic uplift across the Himalayas of central Nepal. Journal of Geophysical Research: Solid Earth, 106(B11), 26561-26591.

Mahesh, P., Gupta, S., Saikia, U., and Rai, S. S., 2015, Seismotectonics and crustal stress field in the Kumaon-Garhwal Himalaya: Tectonophysics, v. 655, p. 124-138.

Malik, J. N., & Mohanty, C. (2007). Active tectonic influence on the evolution of drainage and landscape: geomorphic signatures from frontal and hinterland areas along the Northwestern Himalaya, India. *Journal of Asian Earth Sciences*, *29*(5-6), 604-618.

Miller, J. R. (1991). The influence of bedrock geology on knickpoint development and channel-bed degradation along downcutting streams in south-central Indiana. The Journal of Geology, 99(4), 591-605.

Mitra, G., Bhattacharyya, K., & Mukul, M. (2010). The lesser Himalayan duplex in Sikkim: implications for variations in Himalayan shortening. *Journal of the Geological Society of India*, *75*(1), 289-301.

Montgomery, D. R., & Brandon, M. T. (2002). Topographic controls on erosion rates in tectonically active mountain ranges. Earth and Planetary Science Letters, 201(3-4), 481-489.

Mukherjee S. (2015) A review on out-of-sequence deformation in the Himalaya. In: Mukherjee S, Carosi R, van der Beek P, Mukherjee BK, Robinson D (Eds) Tectonics of the Himalaya. Geological Society, London. Special Publications 412, 67-109.

Mukul, M., Jaiswal, M., & Singhvi, A. K. (2007). Timing of recent out-of-sequence active deformation in the frontal Himalayan wedge: Insights from the Darjiling sub-Himalaya, India. *Geology*, *35*(11), 999-1002.

Nábělek, J., Hetényi, G., Vergne, J., Sapkota, S., Kafle, B., Jiang, M., Su, H., Chen, J., & Huang, B. S. (2009). Underplating in the Himalaya-Tibet collision zone revealed by the Hi-CLIMB experiment. Science, 325(5946), 1371-1374.

Nadim, F., Kjekstad, O., Peduzzi, P., Herold, C., &Jaedicke, C. (2006). Global landslide and avalanche hotspots. Landslides, 3(2), 159-173.

Nennewitz, M., Thiede, R. C., & Bookhagen, B. (2018). Fault activity, tectonic segmentation, and deformation pattern of the western Himalaya on Ma timescales inferred from landscape morphology. Lithosphere, 10(5), 632-640.

Ni, J., and M. Barazangi (1984), Seismotectonics of the Himalayan collision zone: Geometry of the underthrusting Indian plate beneath the Himalaya, J. Geophys. Res., 89, 1147 – 1163.

Niedzielski, T., Migoń, P., & Placek, A. (2009). A minimum sample size required from Schmidt hammer measurements. *Earth Surface Processes and Landforms: The Journal of the British Geomorphological Research Group*, *34*(13), 1713-1725.

Norin, E. (1926). The relief chronology of the Chenab valley. Geografiska Annaler, 8(4), 284-300.

Olley, J., Caitcheon, G., & Murray, A. (1998). The distribution of apparent dose as determined by optically stimulated luminescence in small aliquots of fluvial quartz: implications for dating young sediments. *Quaternary Science Reviews*, *17*(11), 1033-1040.

Ouimet, W. B., Whipple, K. X., Crosby, B. T., Johnson, J. P., & Schildgen, T. F. (2008). Epigenetic gorges in fluvial landscapes. *Earth Surface Processes and Landforms: The Journal of the British Geomorphological Research Group*, *33*(13), 1993-2009.

Preusser, F. (2003). IRSL dating of K-rich feldspars using the SAR protocol: comparison with independent age control. *Ancient tL*, *21*(1), 17-23.

Robert, X., Van Der Beek, P., Braun, J., Perry, C., Dubille, M., & Mugnier, J. L. (2009). Assessing Quaternary reactivation of the Main Central thrust zone (central Nepal Himalaya): New thermochronologic data and numerical modeling. *Geology*, *37*(8), 731-734.

Roberts, H. M. (2007). Assessing the effectiveness of the double-SAR protocol in isolating a luminescence signal dominated by quartz. *Radiation measurements*, *42*(10), 1627-1636.

Robinson, D. M., & Martin, A. J. (2014). Reconstructing the Greater Indian margin: A balanced cross section in central Nepal focusing on the Lesser Himalayan duplex. *Tectonics*, *33*(11), 2143-2168.

Royden, L., & Taylor Perron, J. (2013). Solutions of the stream power equation and application to the evolution of River longitudinal profiles. *Journal of Geophysical Research: Earth Surface*, *118*(2), 497-518.

Scherler, D., Bookhagen, B., Wulf, H., Preusser, F., & Strecker, M. R. (2015). Increased late Pleistocene erosion rates during fluvial aggradation in the Garhwal Himalaya, northern India. *Earth and Planetary Science Letters*, *428*, 255-266.

Schwanghart, W., &Scherler, D. (2014). TopoToolbox 2–MATLAB-based software for topographic analysis and modeling in Earth surface sciences. Earth Surface Dynamics, 2(1), 1-7.

Searle, M. P., Noble, S. R., Cottle, J. M., Waters, D. J., Mitchell, A. H. G., Hlaing, T., &Horstwood, M. S. A. (2007). Tectonic evolution of the Mogok metamorphic belt, Burma (Myanmar) constrained by U-Th-Pb dating of metamorphic and magmatic rocks. Tectonics, 26(3).

Seeber, L., &Gornitz, V. (1983). River profiles along the Himalayan arc as indicators of active tectonics. *Tectonophysics*, *92*(4), 335-367.

Snyder, N. P., Whipple, K. X., Tucker, G. E., &Merritts, D. J. (2000). Landscape response to tectonic forcing: Digital elevation model analysis of stream profiles in the Mendocino triple junction region, northern California. Geological Society of America Bulletin, 112(8), 1250-1263.

Steck, A. (2003). Geology of the NW Indian Himalaya. EclogaeGeolHelv, 96, 147-196.

Stevens, V. L., & Avouac, J. P. (2015). Interseismic coupling on the main Himalayan thrust. Geophysical Research Letters, 42(14), 5828-5837.

Stübner, K., Grujic, D., Dunkl, I., Thiede, R., & Eugster, P. (2018). Pliocene episodic exhumation and the significance of the Munsiari thrust in the north-western Himalaya. *Earth and Planetary Science Letters*, *481*, 273-283.

Thakur, V. C. (Ed.). (1992). Geology of western Himalaya (Vol. 19). Pergamon Press.

Thakur, V. C., Joshi, M., Sahoo, D., Suresh, N., Jayangondapermal, R., & Singh, A. (2014). Partitioning of convergence in Northwest Sub-Himalaya: estimation of late Quaternary uplift and convergence rates across the Kangra reentrant, North India. International Journal of Earth Sciences, 103(4), 1037-1056.

Thiede, R., Robert, X., Stübner, K., Dey, S., &Faruhn, J. (2017). Sustained out-of-sequence shortening along a tectonically active segment of the Main Boundary thrust: The Dhauladhar Range in the north-western Himalaya. Lithosphere, 9(5), 715-725.

Thiede, R. C., Bookhagen, B., Arrowsmith, J. R., Sobel, E. R., & Strecker, M. R. (2004). Climatic control on rapid exhumation along the southern Himalayan Front. Earth and Planetary Science Letters, 222(3-4), 791–806. https://doi.org/10.1016/j.epsl.2004.03.015

Turowski, J. M., Lague, D., and Hovius, N. (2009). Response of bedrock channel width to tectonic forcing: Insights from a numerical model, theoretical considerations, and comparison with field data. *Journal of Geophysical Research: Earth Surface*, *114*(F3).

Vassallo, R., Mugnier, J. L., Vignon, V., Malik, M. A., Jayangondaperumal, R., Srivastava, P., and Carcaillet, J. (2015). Distribution of the late-Quaternary deformation in north-western Himalaya. Earth and Planetary Science Letters, 411, 241-252.

Wadia, D. N. (1934). The Cambrian-Trias sequence of north-western Kashmir (parts of Muzaffarabad and Baramula districts). Records of the Geological Survey of India, 68(2), 121-176.

Webb, A. A. G., Yin, A., Harrison, T. M., Célérier, J., Gehrels, G. E., Manning, C. E., & Grove, M. (2011). Cenozoic tectonic history of the Himachal Himalaya (north-western India) and its constraints on the formation mechanism of the Himalayan orogen. *Geosphere*, *7*(4), 1013-1061.

Wesnousky, S. G., Kumar, S., Mohindra, R., & Thakur, V. C. (1999). Uplift and convergence along the Himalayan Frontal Thrust of India. Tectonics, 18(6), 967-976.

Whipple, K. X., & Tucker, G. E. (1999). Dynamics of the stream-power river incision model: Implications for height limits of mountain ranges, landscape response timescales, and research needs. Journal of Geophysical Research: Solid Earth, 104(B8), 17661-17674.

Whipple, K. X., DiBiase, R. A., & Crosby, B. T. (2013). Bedrock rivers. In Treatise on geomorphology. Elsevier Inc..

Wallinga, J., Murray, A. S., Duller, G. A., & Törnqvist, T. E. (2001). Testing optically stimulated luminescence dating of sand-sized quartz and feldspar from fluvial deposits. *Earth and Planetary Science Letters*, *193*(3-4), 617-630.

Wobus, C. W., Hodges, K. V., & Whipple, K. X. (2003). Has focused denudation sustained active thrusting at the Himalayan topographic front?. *Geology*, *31*(10), 861-864.

Wobus, C., Heimsath, A., Whipple, K., & Hodges, K. (2005). Active out-of-sequence thrust faulting in the central Nepalese Himalaya. Nature, 434(7036), 1008.

Wobus, C., Whipple, K. X., Kirby, E., Snyder, N., Johnson, J., Spyropolou, K., Crosby, B., Sheehan, D & Willett, S. D. (2006). Tectonics from topography: Procedures, promise, and pitfalls. Special papers-geological society of America, 398, 55.

Yadav, R. K., Gahalaut, V. K., Bansal, A. K., Sati, S., Catherine, J., Gautam, P., Kumar, K., and Rana, N., 2019, Strong seismic coupling underneath Garhwal–Kumaun region, NW Himalaya, India: Earth and Planetary Science Letters, v. 506, p. 8-14.

Yin, A., & Harrison, T. M. (2000). Geologic evolution of the Himalayan-Tibetan orogen. Annual Review of Earth and Planetary Sciences, 28(1), 211-280.

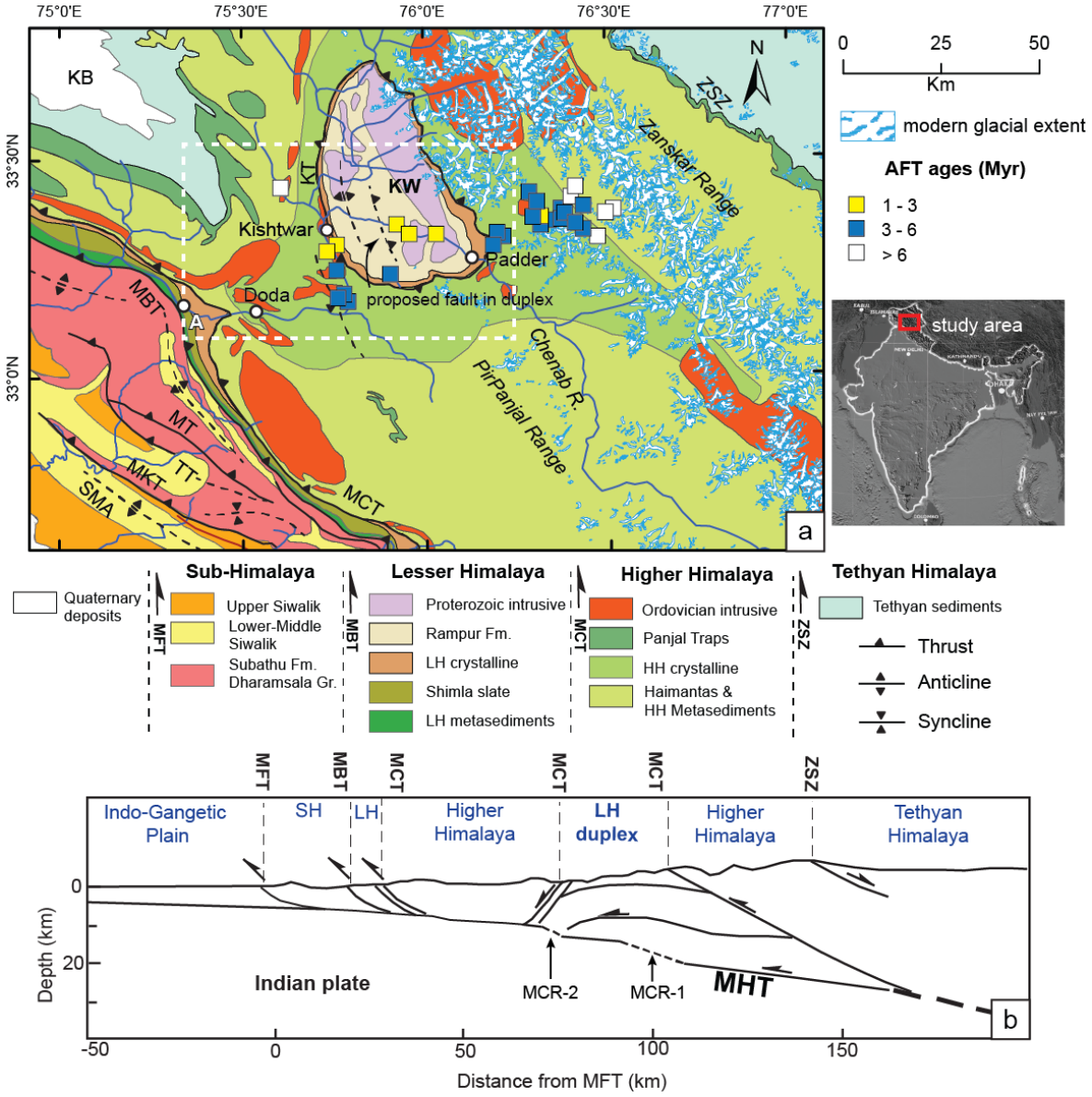

Figure 1: (a) An overview geological map of the western sector of the Indian Himalaya showing major lithology (modified after Steck, 2003 and Gavillot et al., 2018) and existing structures (Vassalo et al., 2015; Gavillot et al., 2018). The tectonic Kishtwar Window (KW) is surrounded by exposure of MCT, locally known as the Kishtwar Thrust (KT), and exposes the Lesser Himalayan duplex. The Lesser Himalayan duplex (LH duplex) forms a west-verging asymmetric anticline. The present-day glacial extent is mapped as per the GLIMS-database. Apatite fission-track (AFT) ages are adapted from Kumar et al., (1995). (b) A schematic cross-section of the NW Himalaya showing the general architecture of the Himalayan orogenic wedge (modified after Webb et al., 2011; Deeken et al., 2011; Gavillot et al., 2018). Note that, beneath the LH Duplex in KW, Gavillot et al., (2018) proposed the existence of at least two crustal ramps (MCR-1 and MCR-2) on the MHT.

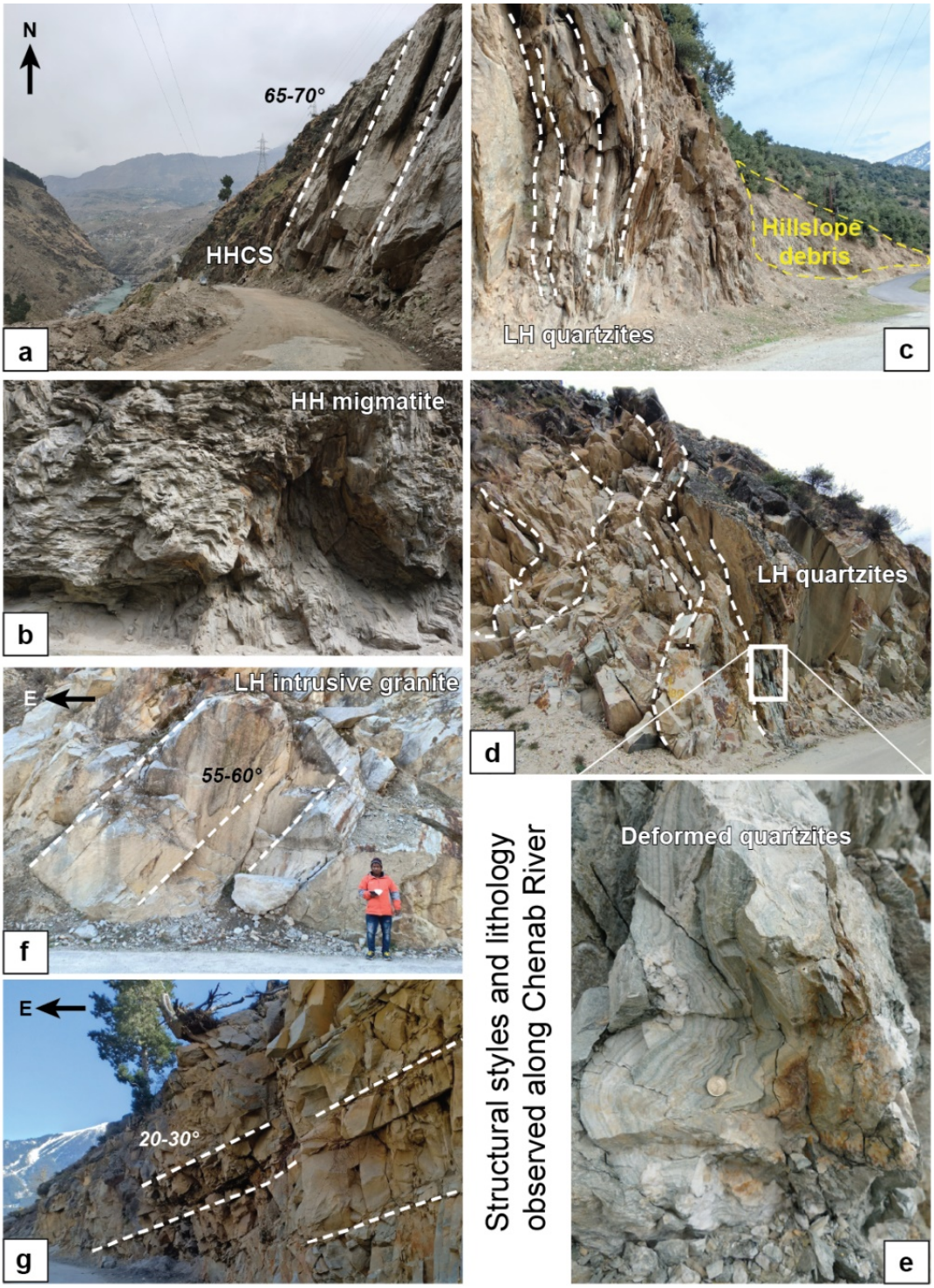

Figure 2: Lithological units and structural orientations observed in the Chenab valley. (a) Steeply-dipping HHCS units near the western margin of the KW. (b) Highly-deformed migmatites at the base of the KT. (c) Sub-vertical quartzite slabs exposed in the frontal horses of the LH Duplex. (d) Highly-deformed granite gneisses at the core of the KW, the hanging wall rocks of the proposed surface-breaking fault (Fig. 8b). (e) A close-up view of the folded and fractured gneiss. (f) Steeply-dipping units of granite gneiss outcropping upstream from the fault-zone. (g) Further upstream from the fault-zone, the bedrocks are gentler in the eastern edge of the KW.

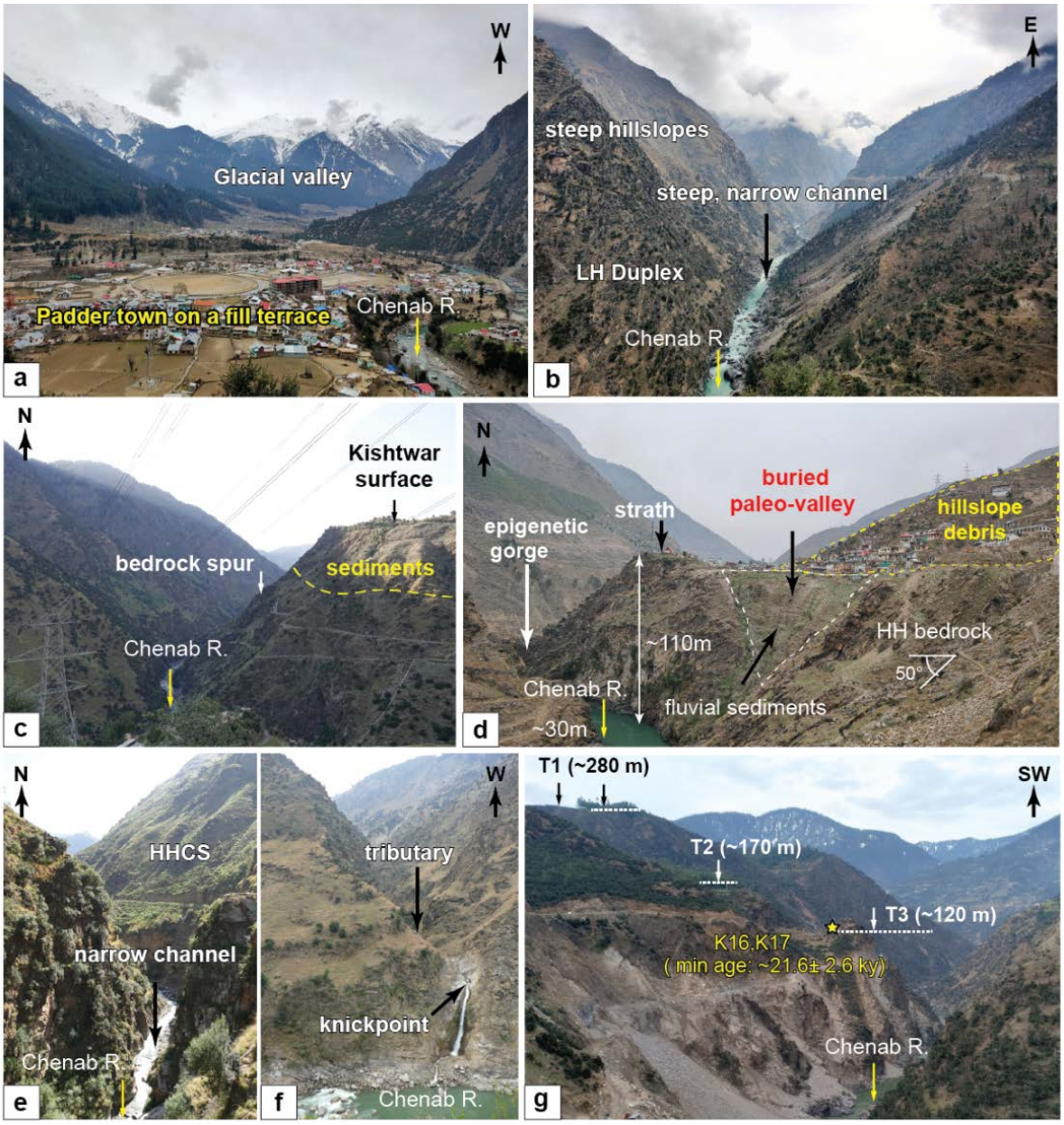

Figure 3: Geomorphic features observed along the Chenab River. (a) 'U-shaped' valley profile at the eastern margin of the KW suggests glacial occupancy in the past. The present-day River incises through the transient sediment storage. Photograph was taken near the town of Padder (cf. Fig.1a). (b) The Chenab River is steep and maintains a narrow channel width through the core of the KW. (c) Fluvial incision observed along the N-S traverse of the Chenab River. Photograph was taken from south of the Kishtwar town. The Kishtwar surface is underlain by ~150-170m thick sediment cover overlying the tilted Higher Himalayan bedrock. The River incised ~240m bedrock in this section. (d) Epigenetic gorge formed along the Chenab River in its' N-S traverse through the HHCS. The town of Drabshalla is built on the hillslope deposits. (e) Chenab River maintained very narrow channel (width: ~20-25 m) through moderately-strong HHCS rocks, suggesting tectonic imprint on topography. (f) Formation of knickpoint at the confluence of the tributary with the trunk stream implying a transient topographic condition. (g) Three levels of strath surfaces observed below the Kishtwar surface. The strath levels are marked as T1 (~280m), T2 (~170m) and T3 (~120m).

OSL dating of fluvial sediments lying above the T3 surface yield a minimum depositional age of ~21.6±2.6 ky.

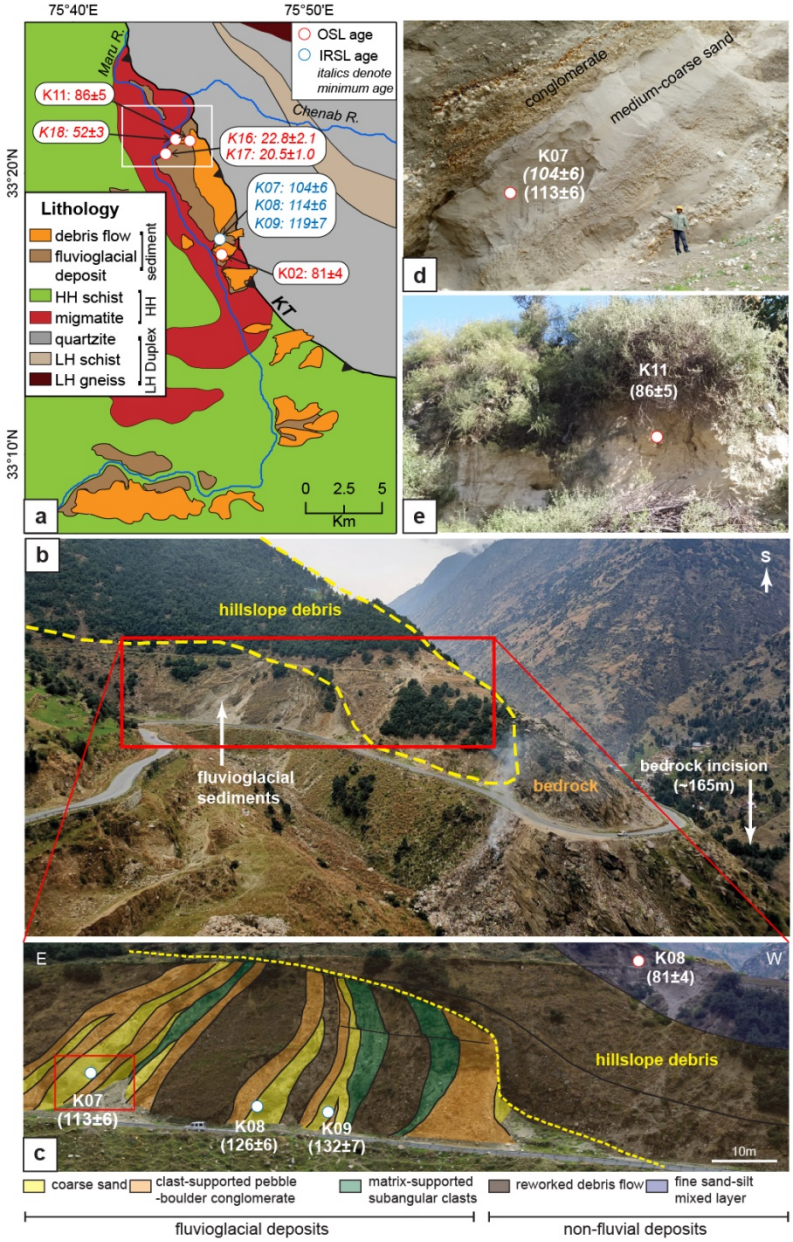

Figure 4: (a) Lithological distribution near the western margin of the KW. Luminescence sample (OSL and IRSL) locations and respective depositional ages (in ky) are shown. Every ample except K16 and K17 are taken above strath level T1. K16 and K17 are taken from above the T3 level. Note that, the ages reported in italics are minimum age estimates. (b) A field photograph from the village Janwas, south of the town of Kishtwar, showing the aggraded sediments lying above the Higher Himalayan tilted bedrock units. (c) IRSL ages (in ky) from the fluvioglacial sediments and OSL age (in ky) from the hillslope debris units suggest the valley aggradation probably started at the transition of the glacial to interglacial phase ~120-130 ky and continued till ~80 ky ago. (d) A close-up view (red rectangle in

fig.4c) of the tilted fluvioglacial sediment layers showing alternate conglomerate and medium-coarse sand layers. (e) A ~3m thick fine sand layer within the hillslope debris yield depositional age of ~86±5 ky. Picture taken near the village Pochal, northwest of the town of Kishtwar.

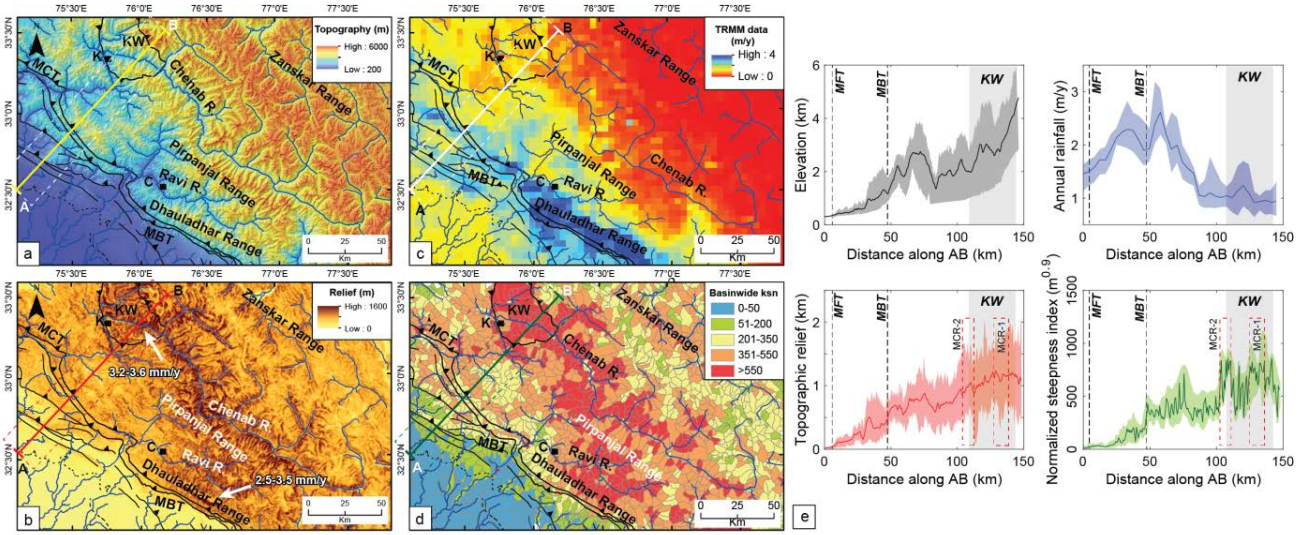

Figure 5: Regional variations in (a) topography, (b) topographic relief (moving window of ~4 km) (c) TRMM-derived rainfall (after Bookhagen and Burbank, 2006), and (d) Basinwide Normalized steepness indices (ksn value) of the region shown dashed box in Figure 1a. (e) Swath profiles (swath window: 50 km) along the line AB (cf. Fig.5a) demonstrate the orogen-perpendicular variations in elevation, rainfall and ksn value. KW is characterized by high elevation, high relief and high steepness, but low rainfall. This suggests that tectonics control uplift and shape of topography not climate.

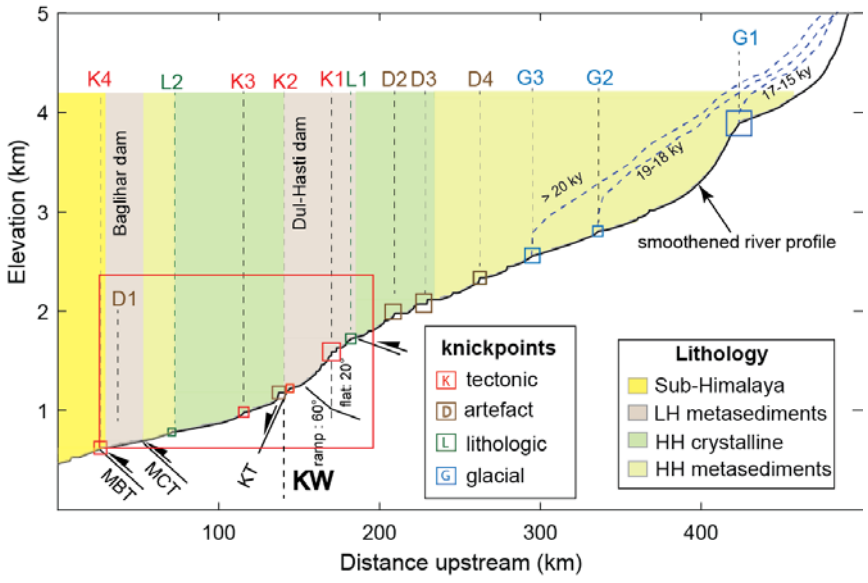

Figure 6: Longitudinal profile of the Chenab River show major changes in channel gradient associated with knickpoints in the upstream. We classified knickpoints on the basis of their genesis. The substrate lithology along the River is shown. Knickpoints caused by glacial occupancy (G1, G2 and G3) are adapted from Eugster et al., (2016), who reconstructed the timing of maximum glaciation and extent of glacial cover in source region of Chenab River basin during the last glacial maximum. These knickpoints highlight the importance of glacial erosion in the high-elevation sectors, especially in the northern tributaries of the Chenab River (For present-day glacial extent cf. Fig.1a). Further in this study, we focused on the area marked by red rectangle.

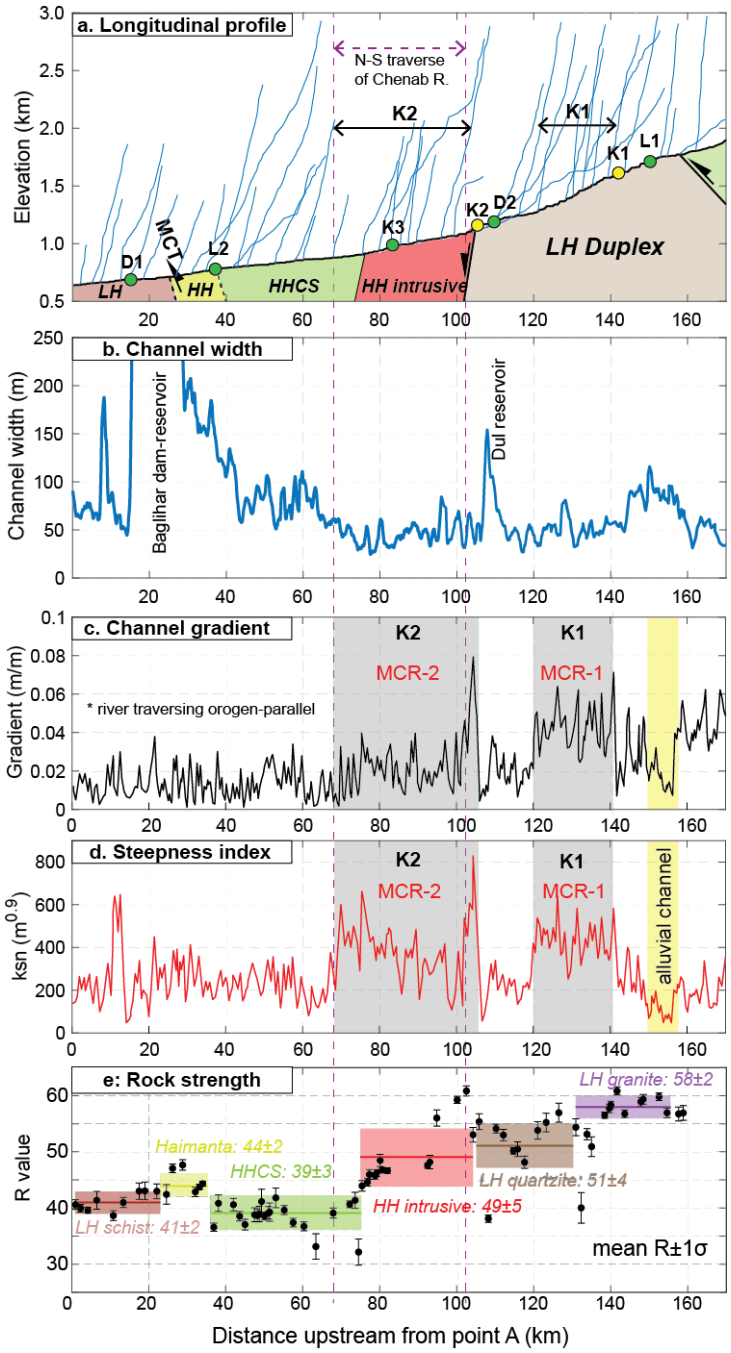

Figure 7: Along-river variations in (a) channel-elevation, (b) channel width, (c) channel gradient, (d) Normalized steepness index, and (e) rock-strength of non-fractured bedrock units (R-value taken by rebound hammer) till 165 km upstream from the MBT (point A, cf. Fig.1a). The mean R-value ± σ for each rock type has been plotted against their spatial extent. We identified two distinct zones (K1 and K2) of high channel gradient and steepness index, which maintain low channel width despite the variable rock strength of the substrate. Knickpoint K3 may have been generated by the formation of the epigenetic gorge along the

N-S traverse of the Chenab River (cf. Fig.3c). Knickpoints L1 and L2 mark the transition of a soft-to-hard bedrock substrate.

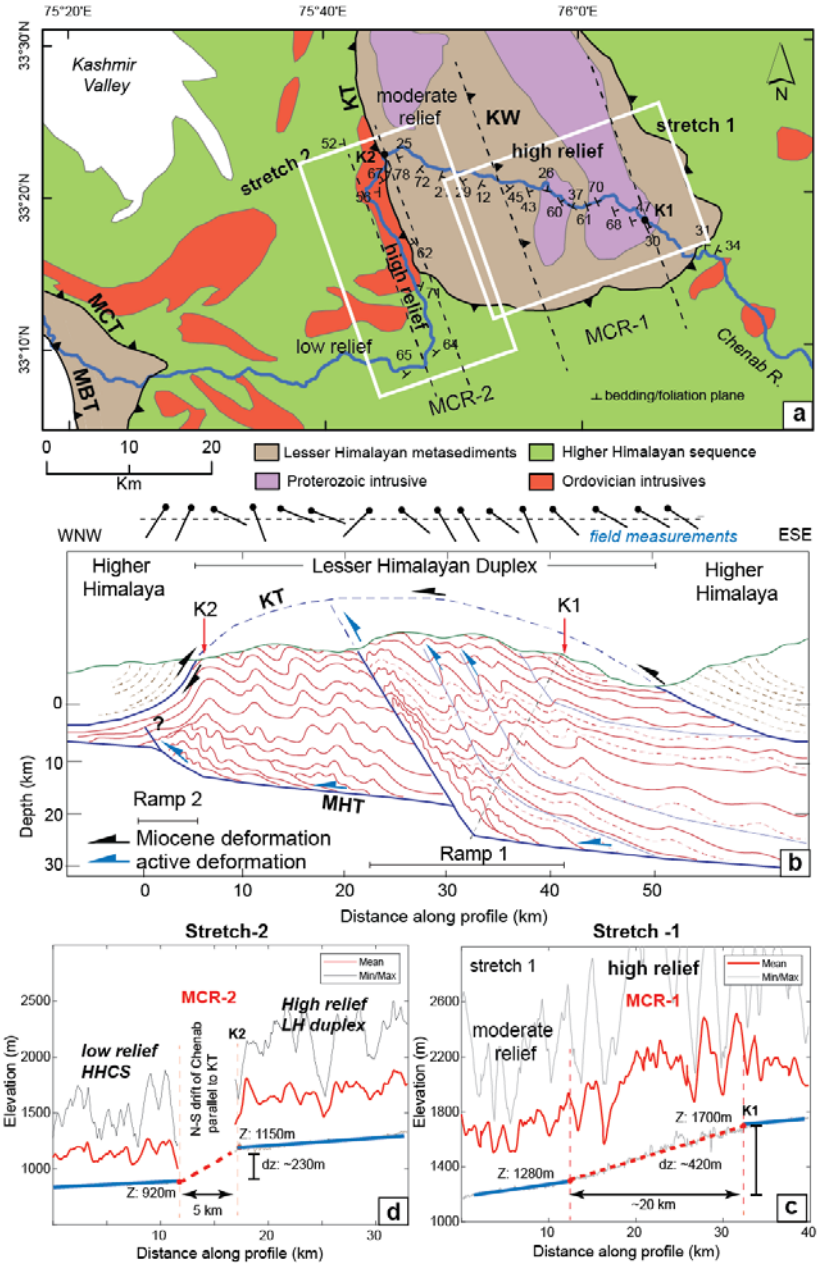

Figure 8: (a) Detailed structural data from the study area showing structural and lithological variations (modified after Steck, 2003; Gavillot et al., 2018). (b) A conceptual drawing of the internal deformation of the LH duplex showing the existing structural variations of the MHT and possible locations of mid-crustal ramps. We assume that two steep stream segment (in the vicinity of knick-zones K1 and K2 – see Fig. 6) refer to ramp segments within the MHT trace. The pervasively folded and fractured LH units at the base of the ramp (cf. Fig. 2e) possibly indicate a surface-breaking fault within the LH duplex. Sustained uplift of the

hanging wall of the proposed fault is expressed by the higher topographic relief, narrowing of the channel and River steepening on the hanging wall. Structural variations on the hanging wall impart differential uplift, marked by a quasistatic knickpoint K1 at the transition from the flat to the ramp of the fault. 3-km-wide topographic swath profiles are drawn across the steep stream segments K1 (fig.8c) and K2 (fig.8d). The orthogonal profile projection method has been used in the case of K2 (cf. fig.7) to identify the width of the steep segment.

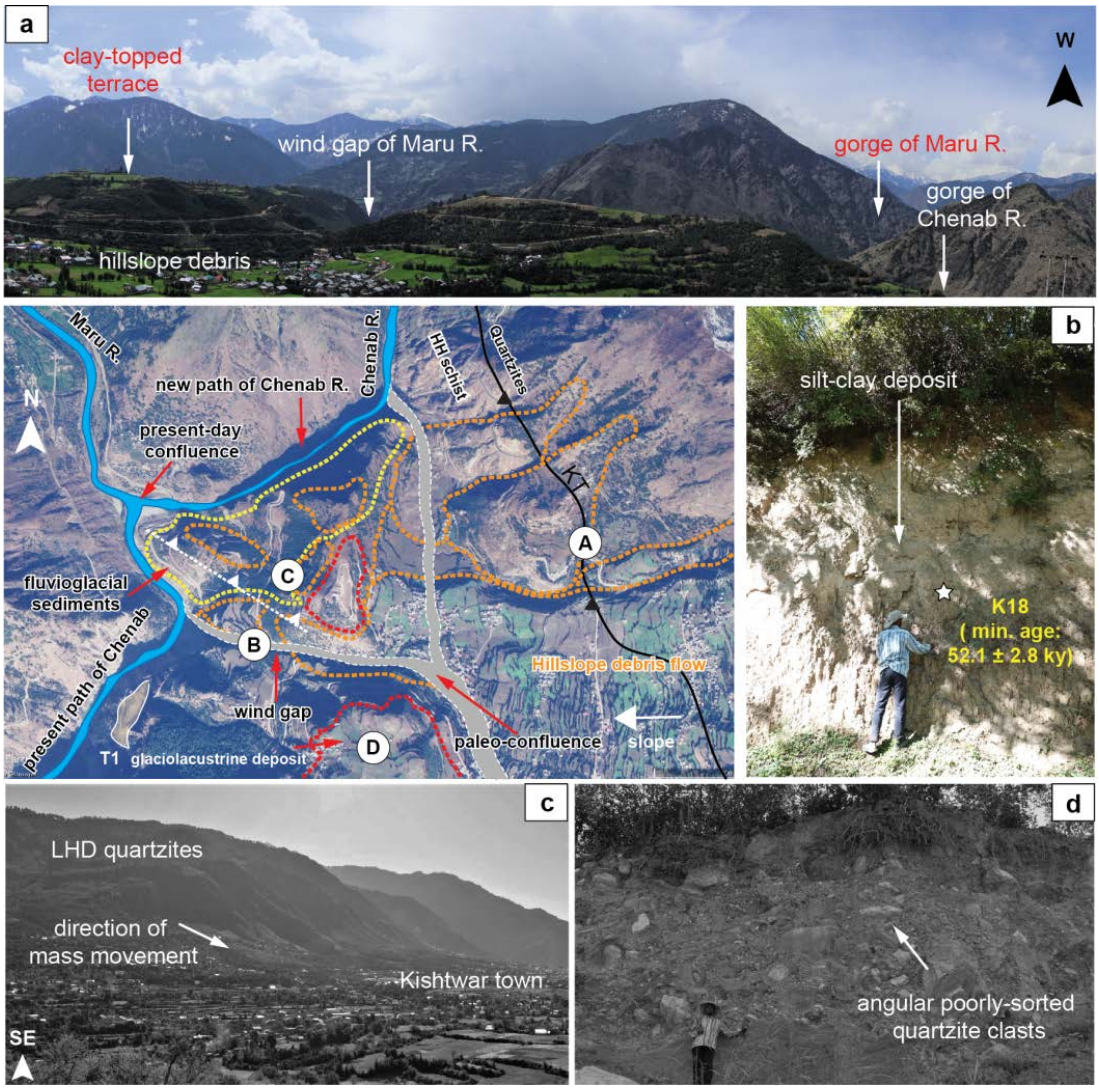

Figure 9: A satellite image of the northern Kishtwar town showing the present-day flow-path of the Chenab River. Hillslope debris originated from the steep frontal horses of the LH duplex (white quartzite rocks) and was deposited over fluvioglacial and glaciolacustrine sediments and Higher Himalaya schists bedrock exposed below in the Kishtwar valley. Massive hillslope sediment flux impeded the paleo-drainage system leaving behind the paleo-valley of the tributary, the Maru River. Our interpretation of the paleo-drainage is marked in a white dashed line. (a) A view of the Kishtwar surface from the western margin of the KW

showing present-day gorge of the Chenab River and its tributary. The wind-gap (paleo-valley) of the tributary is visible. (b) Thick clay-silt deposit in the wind-gap suggests abandonment of river-flow. The OSL sample is saturated and hence only denotes the minimum age of valley abandonment/ hillslope debris flow. (c) Overview picture of the frontal horses of the LH duplex and the direction of debris flow towards the Kishtwar town. (d) Angular, poorly-sorted clasts and boulders were observed at the base of the debris flow unit near the village of Pochal, north of the Kishtwar town. The white quartzites of LH are exposed in the vicinity of the Kishtwar Town (see satellite image) – only the eastern valley flank can have collapsed in the past.

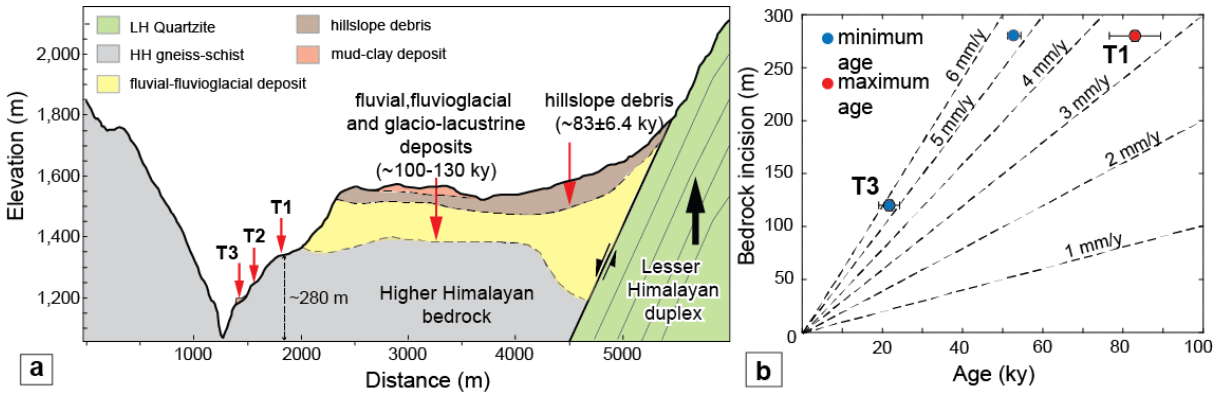

Figure 10: (a) A topographic and geomorphic profile across the Chenab valley drawn over the Kishtwar Town. The valley aggradation by fluvioglacial and hillslope debris sediments was succeeded by a fluvial incision which penetrated through the unconsolidated sediments of thickness ~140-150m and incised Higher Himalayan bedrock by ~280±5 m, leaving behind at least three recognizable strath surfaces with a thin late Pleistocene sediment cover. The three strath surfaces are at 280±5 m (T1), ~170 m (T2), and ~120±5 m (T3) heights from the present-day River. We assume that the present-day bedrock gorge has been carved since the deposition of the glaciolacustrine sediment deposits (~100-130 ky) and the hillslope debris (~90-80 ky) onto former fluvial strath surface of Higher Himalayan Bedrock. The width of the fluvial strath surface where the Kishtwar Town is located indicates that the river network had been dammed earlier too. (b) Graphical representation of mean bedrock incision rates since 80 ky. Age constraints for T3 are shown in Fig. 4a. We propose a minimum and a maximum bedrock incision rate of 3.1-3.5 mm/y and 5.2-5.6 mm/y, respectively. Rapid bedrock incision along the N-S traverse of the Chenab River may imply sustained exhumation over the proposed mid-crustal ramp of the MHT.

Tables

Parameter	flat 1	MCR-1	% change	ratio ramp 1:flat 1	flat 2	MCR-2	% change	ratio ramp 2:flat 2
average channel gradient (m/m)	0.006	0.021	250.00	3.5	0.01	0.046	360	4.60
average channel width (m)	70	45	-35.71	0.6	55	42	-24	0.76
*Specific stream power (SSP)	0.000086	0.000467	444.44	5.4	0.000182	0.001095	502	6.02

* SSP calculated by assuming uniform-discharge (Q)

Table 1: Calculations of change in specific stream power (SSP) values across the ramp and the flat segments beneath the LH Duplex. We used a uniform discharge for SSP calculation.

Sample type	Sample name	Lat (°)	Long (°)	U (ppm)	Th (ppm)	K (%)	water (%)	Dose rate (Gy/ky)	De (Gy)	OD (%)	Age (ky)	fading correction	Corrected age (ky)
using central age model													
OSL	K02	33.29607	75.77619	3.8	7.2	0.46	6.1	1.74±0.02	141±8	19.5	81.1±4.6		
OSL	K11	33.3535	75.74649	3.1	12.7	2.41	6	3.97±0.09	341±19	16.8	85.7±5.1		
IRSL	K07	33.2778	75.76922	3.3	13.8	2.31	5.3	4.67±0.22	489±29	16.8	104.5±5.9	0.89	113±6
IRSL	K08	33.2778	75.76922	3.5	16.9	1.97	5.6	4.61±0.23	528±38	20.5	114.4±6.3		
IRSL	K09	33.2778	75.76922	3.3	12.2	1.98	4.8	4.29±0.20	510±42	18.1	119.2±6.8	1.11	132±7
using minimum age model													
OSL	K16	33.34873	75.73324	3.5	16.8	2.03	7.5	3.95±0.1	90±8	40	22.8±2.1		
OSL	K17	33.34873	75.73324	3.4	18	2.17	10.5	3.96±0.11	81±3.5	46	20.5±1.0		
saturated sample													
OSL	K18	33.35176	75.74325	3.3	18.7	2.61	4.5	4.36±0.13	227±14		52.1±2.8		

0

1 Table 2: Sample locations, elemental concentrations, dose rates, equivalent doses and age estimations for sand samples from Kishtwar valley.

2

3

4